

Efficient Time Evolution of 2D Open-Quantum Lattice Models with Long-Range Interactions using Tensor Networks

J. Dunham^{1, 2, 3, *} and M. H. Szymańska¹

¹Department of Physics and Astronomy, University College London, Gower Street, London, WC1E 6BT, United Kingdom

²London Centre of Nanotechnology, 9 Gordon St, London WC1H 0AH, United Kingdom

³Center for Theoretical Physics, Polish Academy of Sciences, Al. Lotników 32/46, 02-668 Warsaw, Poland

(Dated: November 20, 2025)

Simulating many-body open quantum systems is an extremely challenging problem, with methods often restricted to either models with nearest-neighbor interactions or semi-classical approximations. In particular, modeling two-dimensional systems with realistic long-range interactions, in addition to dissipation, is of vital importance to the development of modern quantum computing and simulation platforms. In this paper, we present a construction of the time-evolution operator, as a projected entangled pair operator (denoted tePEPO), that can be used to evolve a tensor network ansatz through time. Interactions beyond nearest-neighbor, including interactions between sites not collinear in the lattice, can be represented efficiently as a tePEPO. Furthermore, we obtain approximations to realistic radial long-range interactions decaying with a power-law, that give accurate results with small tePEPO bond dimension. Finally, we consider a physical example of a Rydberg atom Hamiltonian with long-range dipolar interactions, and show evidence of a dipole-dipole blocking effect in presence of dissipation. This work demonstrates the applicability of tensor networks to two-dimensional systems widely studied in experiments, but previously inaccessible to non-semi-classical methods.

I. INTRODUCTION

Precise control of arrays of interacting quantum objects is a task central to the development of modern quantum technologies such as quantum computers and simulators. Ideally, these *many-body* quantum systems would be perfectly isolated from their environment, operating as closed systems; however in the real world this is practically impossible to achieve. While strides have been made in mitigating decoherence caused by external effects [1] in such *open* quantum systems, many novel phenomena can actually emerge from the interplay between a systems coherent evolution, external drive, and dissipative effects, with no counterpart found in closed systems. In addition, many-body open quantum systems have been proposed as a computation resource [2], for quantum state preparation [3–6], to aid quantum error correction [7], and as store of energy in the form of a quantum battery [8], among others. Furthermore, the rapid advancement in engineering affords us unparalleled control of such driven-dissipative effects in platforms such as exciton-polaritons [9], ultracold atoms [10], and circuit- and cavity-QED [11, 12], to name a few.

In light of this, the task of modeling many-body open quantum systems is vital to the development of quantum technologies in both the near- and long-term, while still remaining one of the most formidable challenges in computational physics. Many-body quantum systems occupy a Hilbert space that is exponentially large with respect to the number of particles (for example), precluding an exact simulation of more than only a few. Furthermore, the state of an open quantum system is typically

expressed as a *density matrix*, leading to an additional quadratic penalty compared to the state vector description of a closed system. In some cases, exact solutions have been found [13, 14], but these are limited, and while analytical techniques such as the Keldysh formalism [15] can provide insights beyond the mean-field approximation [16], for the most part, sophisticated numerical techniques must be employed. Moreover, the wealth of numerical methods in the literature of closed systems are not always transferable, necessitating the development of techniques specific to open quantum systems.

To this end, a variety of numerical approaches have emerged. Variational Monte Carlo methods [17] have been used to find steady-states and dynamics of Lind-

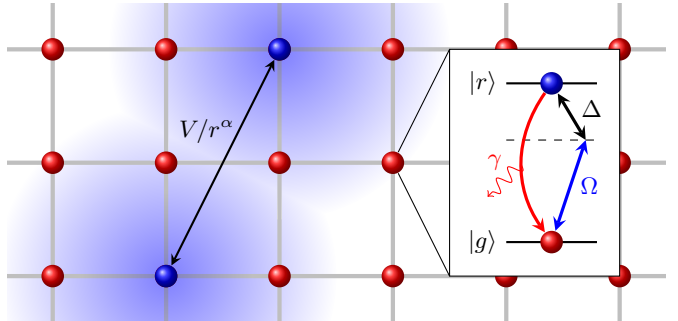


FIG. 1. **Example of a many-body open quantum system.** Atoms in excited Rydberg states $|r\rangle$ with strong, long-range repulsive interactions decaying as a power law $r^{-\alpha}$, typically of van der Waals $\alpha = 6$ or dipolar $\alpha = 3$ form. Atoms are promoted from the ground state $|g\rangle$ to a highly-excited Rydberg state $|r\rangle$ via a laser drive with frequency Ω and detuning Δ . Atoms can then decay $|r\rangle \rightarrow |g\rangle$ incoherently at a rate γ .

* jdunham@flatironinstitute.org

blad equations using a neural network [18–22], and more recently, a tensor network ansatz [23, 24]. Unfortunately, as discussed in Ref. [17], the complex-valued eigenvalues of the associated Liouvillian super-operator can, in some cases, lead to the infamous sign problem [25] in such methods. Methods using the phase space representation of the density matrix, such as the truncated Wigner approximation [26–28] and Positive-P are highly scalable, however the former is semi-classical, failing to capture all physical aspects of bosonic systems [29], and the latter, while particularly suited to system with dissipation [30], has yet to be formulated for spins.

For closed systems, *tensor network methods*, such as the celebrated density matrix renormalization group (DMRG) algorithm [31, 32], have been enormously successful in the treatment of strongly-correlated many-body quantum lattice models. Such methods represent the quantum state as a network of tensors, which geometry is intrinsically related to entanglement structure of the underlying state. Tensor networks then parameterize an exponentially smaller, physically relevant corner of the total Hilbert space. The dimension of the indices that connect these tensors in the network, known as the bond dimension, acts a parameter that controls the expressibility of the ansatz. For open quantum systems, methods based on tensor networks are attractive as they tend to not impose additional approximations on the equations of motion, in contrast to semi-classical approaches, and allow direct access to the density matrix. This enables one to compute entanglement measures, such as mutual information negativity, not necessarily available to phase-space methods. Moreover, increasing the bond dimension allows one to, in principle, systematically improve the simulation by allowing the ansatz to capture more of the quantum correlations and entanglement present in the system.

For the most part, the majority of tensor network works in this field have been limited to one-dimensional systems [33–42]. For two-dimensional open quantum systems, studies are scarce, and limited to nearest-neighbor interactions [43–45]. They employ the two-dimensional time-evolving block decimation (TEBD) [33, 46–48] algorithm to solve the Lindblad master equation, a method most applicable to models with only nearest-neighbor interactions. Studies moving beyond the nearest-neighbor case are rarer still; the extent that tensor networks can be applied to Lindblad time evolution beyond the nearest-neighbor case remains largely unexplored. Some progress has been made to this end, albeit restricted to one-dimensional systems: long-range interactions have been modeled on finite chain using tree-tensor networks (TTN) [39, 41], however TTN are not able to capture the two-dimensional area-law, severely limiting the expressibility of such an ansatz. Recently, Monte Carlo with a matrix-product state ansatz capable of studying long-range interactions was proposed [23, 24], however this requires contracting finite-sized two-dimensional tensor networks, a task in the $\#P$ complexity class [49].

Evidently, the study of open quantum systems with long-range models is an under-explored area of research, despite their relevance to current experimental platforms in quantum computing and simulation [50–52]. Furthermore, it was shown using a variational approach that a full treatment of the long-range tails of dissipative model gives significant corrections compared to considering an effective short-range model [53]. In light of this, the contribution of this paper is the following: we present a recipe for constructing tensor network representations of time-evolution operators for two-dimensional lattice models with interactions beyond nearest-neighbor. This represents a generalization from one dimension to higher dimensions of what are known as the W^I and W^{II} methods [54], which are described in more detail later, and a partial generalization of the associated higher-order cluster expansions [55]. The resulting tensor network time-evolution operators take the form of a projected entangled pair operator (PEPO), and are denoted time-evolving PEPO (tePEPO). The constructed operators can then be used to evolve an infinite projected entangled pair operator (iPEPO) representation of the density matrix through time via a series of apply-and-truncate steps.

We find that realistic 2D power-law interactions can be achieved by considering sums of Gaussian terms, each representable by tePEPO, in analogy to approximations of 1D power-law with sums of exponential [56]. Moreover, we show that good agreement with exact solutions can be achieved with only a modest number of terms in this summation. This then enables the simulation of long-range models, which short-range equivalents prove difficult to simulate with existing tensor network method under equivalent approximations, thus demonstrating an increase in the applicability of such methods to problems in many-body quantum physics. The primary motivation and subsequent application of the methods in this paper is to the Markovian evolution of an open quantum systems, however the construction of the tePEPO is generic and also applicable to real and imaginary time evolution of closed systems.

The paper is structured as follows. We first provide some additional technical context to this work in Sec. II. In Sec. III, we introduce the recipe used to construct two-dimensional tensor-network operator representations of the size-extensive approximation to the time-evolution [54], henceforth denoted the tePEPO. In Sec. IV, we then describe how to approximate interactions decaying with a power-law as a sum of Gaussian functions, which have tePEPO representations. Sec. V presents an efficient algorithm that solves for the time dynamics of the Lindblad equation by repeatedly applying a tePEPO to a iPEPO density matrix ansatz. To benchmark, this algorithm is then applied to an exactly solvable dissipative Ising model in Sec. VIA 1, where it is shown to give accurate results beyond mean field in the strongly dissipative regime. We also show convergence beyond the exactly solvable regime of this model

in Sec. VI A 2. Finally, a dissipative Rydberg Hamiltonian with dipolar interactions is considered in Sec. VI B, where we show the characteristic dipole-dipole blockade effect. We conclude with a discussion, and suggestions of future research directions.

II. BACKGROUND

This paper considers the problem of developing tensor network methods capable of simulating the time-evolution of long-range interacting systems. While readily applicable to real- and imaginary-time evolution of closed systems, we are interested in open quantum system obeying the following Markovian master equation ($\hbar = 1$):

$$\frac{d\rho}{dt} = \mathcal{L}(\rho) = -i[H, \rho] + \mathcal{D}(\rho), \quad (1)$$

known as the Gorini–Kossakowski–Sudarshan–Lindblad (GKSL) equation [57]. The Hamiltonian H of the system governs the coherent dynamics of the quantum state ρ , and the dissipator \mathcal{D} , which models the system-environment coupling,

$$\mathcal{D}(\rho) = \sum_k L_k \rho L_k^\dagger - \frac{1}{2} \left(L_k^\dagger L_k \rho + \rho L_k^\dagger L_k \right), \quad (2)$$

is defined in terms of a set of often-phenomenological jump operators $\{L_k\}$. The solution to equation (1) is then the family of completely-positive trace-preserving (CPTP) maps obtained via exponentiation of the Liouvillian super-operator \mathcal{L} , i.e.

$$e^{t\mathcal{L}} : \rho(0) \mapsto \rho(t). \quad (3)$$

Specifically, we seek a tensor network operator representation of (3) for two-dimensional lattice systems with interactions *beyond* the simple nearest-neighbor case. It is therefore useful to provide a summary of the major technical progress made to this end, and highlight some limitations of existing approaches.

In one-dimension, beyond the context of open quantum systems, interactions decaying with the exponential of distance admit efficient representations as matrix product operator (MPO), which can then be used as a basis to approximate other decay functions [56, 58]. This idea was applied to time dynamics in a size-extensive way by employing techniques from finite-state automata [54, 58]. By extending the cluster expansion approach [59], this idea was generalized further: [55] presents an algorithm that generates an extensive time-evolution matrix product operator of arbitrary order and, through a series of extension and compression steps, can be made optimal in terms of the operator bond-dimension. Provided the operator can be written as an MPO in so-called *regular form* [60], the algorithms in [55] can be applied. The generalization to Lindblad dynamics is straightforward via vectorization [38] and is of particular interest as

completely-positive and trace-preserving (CPTP) Trotter decompositions have not been found beyond second order [36].

Such MPOs can be applied to the two-dimensional problem by Trotterizing over each axis direction allowing one to simulate models with interactions between collinear sites, i.e. between sites with either the same x or y lattice coordinate. These so-called axial interactions, occurring between collinear sites on the lattice, are present in the axial [61, 62] and biaxial next-nearest neighbor Ising models (ANNI and BNNI respectively) commonly studied in the context of frustrated quantum magnetism [63]. Axial long-range interactions, decaying with an inverse power law of distance have also been studied appearing in the context of classical spin lattices and the quantum-classical correspondence [64].

Including interactions between diagonal sites is trickier, requiring a more sophisticated treatment. Next-nearest neighbor (NNN) terms have been accounted for in the finite temperature context, using the so-called next-nearest neighbor update, first considered with application to fermions [65] and later to the classical J_1 - J_2 Heisenberg model [66, 67], where this method has been associated with problematic, fictitious breaking of C_{4v} symmetries. In addition, extending beyond NNN interactions requires increasing unit-cell sizes, quickly becoming impractical.

As for long-range interactions, one proposal couples a finite-state machine PEPO to the partition function of a statistical physics model with a two-point correlation function decaying algebraically with Euclidean distance [68, 69]. However, an extension to time-evolution appears problematic at first glance as it is not obvious how n -point correlation functions can be turned into the required products of two-point correlation functions. Ref. [70] introduce the generalized matrix product operator (gMPO) capable of representing two-dimensional long-range interactions by fitting to Gaussian basis of functions. This method was subsequently applied to the problem of finding the ground state phase diagram of a Rydberg atom array [71], however constructing gMPO forms of time-evolution operators, if possible, is likely represent a significant degree of technical work.

III. CONSTRUCTION OF THE CLUSTER TIME-EVOLUTION OPERATOR

Generally, the goal is to simulate the real or imaginary time evolution of quantum many-body systems defined on a two-dimensional lattice Λ who's mixed-state $\rho(t)$ at time t in the Hilbert space \mathcal{H} is represented by a tensor network ansatz. We will consider the specific case where the time-evolution is generated by an operator \mathcal{G} such that evolution from an initial state $\rho(0)$ is given by a dynamical map of the form:

$$e^{\tau\mathcal{G}} : \rho(0) \mapsto \rho(\tau). \quad (4)$$

of which Lindblad time evolution (3) is a special case.

It remains to construct efficient tensor network operator approximations to (4). We consider specifically a subset of generators \mathcal{G} that can be written in the following form:

$$\mathcal{G} = \sum_{v_1, v_2 \in \Lambda} \left(\sum_{k=1}^{k_{\max}} g_{v_1 v_2}^{[k]} \right) + \sum_{v \in \Lambda} g_v^{[0]}, \quad (5)$$

where the notation $\hat{X}_{v_1 \dots v_n}$ denotes an n -body operator on \mathcal{H} acting as \hat{X} on the subspace of lattice sites $v_1, \dots, v_n \in \Lambda$, and the identity elsewhere, i.e. (5) describes operators formed as sums of at most 2-body terms.

Our goal to find an approximation to the time-evolution operator (4) that has an efficient representation as a tensor network. To simplify the explanation, we will consider the case where the generator \mathcal{G} is the Hamiltonian H of a quantum system, i.e. $\mathcal{G} := H$ in (4) with $\tau := -it$ for real time evolution to a time t . The extension to Lindblad time evolution is deferred to Sec. V.

A. Extensive Expansion

A naive finite order expansion of the time evolution operator (4) in increasing powers of H results in an error intensive in the size of the system N , i.e. the number of neglected terms in the expansion *per site* depends on the system size. However, by including all terms of higher order (up to infinite order) that do not overlap, the neglected terms per lattice site becomes independent of the system size. Specifically, Let $H^{(j)}$ be a local term in a Hamiltonian H with support on a finite subset of the lattice $\lambda_j \subset \Lambda$, then the tuples of indices $I_n = \{j_1, j_2, \dots, j_n \in \Lambda \mid \lambda_i \cap \lambda_j \cap \dots = \emptyset\}$ define tuples of n terms in the Hamiltonian whose support do not overlap. The decomposition:

$$e^{\tau H} \approx 1 + \tau \sum_{(j) \in j_1} H^{(j)} + \tau^2 \sum_{(j, k) \in j_2} H^{(j)} H^{(k)} + \dots, \quad (6)$$

is then size extensive and thus well defined in the thermodynamic limit [54], having $\mathcal{O}(N\tau^2)$ neglected terms. For certain one-dimensional Hamiltonians, the expansion (6) can be represented as a MPO by appealing to the finite state machine (FSM) picture of the Hamiltonian [58, 72], and performing the following ‘loopback’ procedure [55]: each FSM path from the initial state to the final state generates a single term in the Hamiltonian; to generate *products* of terms, one should map the final state of the FSM back to the initial state. This then allows an additional term to be generated in the product-of-terms that itself forms a term in the expansion (6). An n -th order term in (6) is formed from n repetitions of the FSM assuming one multiplies by a factor of τ at each repetition.

This loopback procedure generates what is referred to as the first-order W^I approximation, corresponding to the

| Rule | Index (e, s, w, n) | Value | Rule type |
|------|---------------------------|---------------------------|-----------|
| | (0, 0, 0, 0) | $\mathbb{1}$ | identity |
| | (0, 0, 0, 0) | $-i\hat{D}$ | D |
| | (1, 0, 0, 0) | $J_1 \hat{C}$ | C |
| | (0, 0, 0, 1) | $J_1 \hat{C}$ | C |
| | (0, 0, 1, 0) | $-i\hat{B}$ | B |
| | (0, 1, 0, 0) | $-i\hat{B}$ | B |
| | (1, 1, 0, 0) | $J_2 J_1^{-1} \mathbb{1}$ | A |
| | (0, 1, 2, 0) | $J_2 J_1^{-1} \mathbb{1}$ | A |
| | (2, 0, 0, 0) | $-i\hat{B}$ | B |

TABLE I. Example of non-zero finite signaling agent (FSA) rules for the real time-evolution of the J_1 - J_2 Ising-type Hamiltonian (8), excluding the Hermitian conjugate (h.c.) terms. Including the rules obtained via swapping \hat{C} and \hat{B} in the listed C- and B-type rules gives the h.c. terms. The bond dimension of the resulting tePEPO operator is $\eta_h = 5$ on the horizontal direction and $\eta_v = 3$ on the vertical direction, or $\eta_h = 3$ and $\eta_v = 2$ for the special case of $\hat{C} = \hat{B}$. After including the correct prefactor listed in Table II depending on whether one wishes to generate the W^I or W^{II} approximation, the operator generated by the tePEPO is the sum over all the valid tilings of the listed rules. Note, this specific combination of rules is not unique.

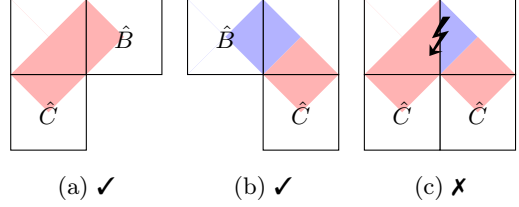


FIG. 2. Examples of two terms (a) and (b) in the Hamiltonian (8) that are accepted by the finite signaling agent (FSA) and another term (c) not in (8) that is correctly rejected due to the additional (blue) level. This term would incorrectly be included in the sum had the blue level been replaced by the red level.

expansion (6). It can be modified further to also include all second-order terms that overlap exactly once [55], resulting in an improved but still first-order operator known as the W^{II} approximation. For details on how to generate such time-evolution operators in MPO form, as well as analogous operators of arbitrary order, we refer to Ref. [55] and the algorithms therein.

| Rule type | W ^I | W ^{II} | | | |
|------------|----------------|-----------------|------|------------------|----------------------|
| | | id | A | B \vee C | D |
| id | 1 | 1 | 1/2 | $\sqrt{\tau}/2$ | $\tau/2$ |
| A | 1 | | 1/2! | $\sqrt{\tau}/2!$ | $\tau/2!$ |
| B \vee C | $\sqrt{\tau}$ | | | $\tau/2!$ | $\tau\sqrt{\tau}/2!$ |
| D | τ | | | | $\tau^2/2!$ |

TABLE II. Prefactor required when constructing products of intersecting rules based on rule type. The table is symmetric. This combination of prefactors is not unique, but is convenient to avoid breaking any symmetry between lattice directions.

B. Finite Signaling Agents

We now describe how to construct the W^I and W^{II} operators in two-dimensions in terms of the finite signaling agent (FSA) generalization of the FSM picture. Suppose for simplicity that Λ is a two-dimensional square lattice. Let \mathcal{H} be the Hilbert space of a many-body quantum system defined on Λ . Now associate to each edge in the lattice an integer, denoted a *signal*, such that for each vertex v there is a tuple of signals, (e, s, w, n) where $e, s, w, n \in \{0, \dots, l-1\}$, defining the signal on each of the 4 edges incident to v (denoted here using the cardinal directions). Let \hat{O} be an operator, acting on \mathcal{H} , of the form

$$\hat{O} = \bigotimes_{v \in \Lambda} \hat{X}^{[v]} \quad (7)$$

such that for all $v \in \Lambda$ the operator $\hat{X}^{[v]}$ is determined by the specific combination of signals on the edges incident to v . If one constructs the operator-valued tensor \hat{X}_{eswn} (where for simplicity we have imposed translational invariance $\hat{X}_{eswn}^{[v]} = \hat{X}_{eswn} \forall v \in \Lambda$), then the corresponding projected entangled pair operator generated by \hat{X}_{eswn} is precisely the sum of the operators \hat{O} that would result from every possible combination of signals assigned to all the edges in the lattice.

This is largely trivial until we impose that $\hat{X}_{eswn} = \hat{0}$ for some combinations of (e, s, w, n) . If any of the vertices receives such a combination, then immediately $\hat{O} = \hat{0}$, and we say the term \hat{O} is *rejected*. All it takes is one such operator in the tensor product (7) to force the term to be rejected. We say that the map $(e, s, w, n) \rightarrow \hat{X}$ defines a FSA *rule*. By carefully choosing the non-zero rules, or in other words, elements of the tensor \hat{X}_{eswn} , one can engineer the resulting sum of non-rejected terms to coincide with the cluster expansion (6) of the desired Hamiltonian, provided we make sure that the rules also accommodate for the correct prefactor of τ^n , which will be described shortly.

Note, at a minimum one must have the zero'th order term $\mathbb{1}$ in (6) so no matter the Hamiltonian, one must have the rule $\hat{X}_{0000} = \mathbb{1}$. This is denoted the background or *identity* rule. We also require that all accepted \hat{O}

Input: Hamiltonian H in the form of FSA rules stored as the rank- z tensor R , where z is the coordination number of the lattice.

Output: Tensor P who's network defines the W^{II} approximation to the time evolution generated by H .

```

1: procedure INCLUDEOVERLAPPING( $R$ )
2:    $I_R \leftarrow$  indices of  $R$ 
3:    $P \leftarrow$  tensor of zeros with indices  $I_R$ 
4:   for  $a \in I_R, b \in I_R$  do
5:     if any  $a[n] \neq 0 \wedge b[n] \neq 0$  for  $n \in [1, z]$  then
6:       skip
7:     else
8:        $c \leftarrow a + b$ 
9:        $\tau \leftarrow$  prefactor of  $R[a] \times R[b]$   $\triangleright$  From Table II
10:       $P[c] \leftarrow P[c] + \tau R[a]R[b]$ 
11:    end if
12:   end for
13:   return  $P$ 
14: end procedure

```

ALGORITHM 1. Generate the W^{II} approximation to a Hamiltonian defined in terms of FSA rules.

represent a valid product of complete terms in H . To enforce this, it is useful to place each rule in one of four categories: C-type rules define the start, or *head* of a given term in H ; similarly, B-type rules define the end, or *tail*; rules of A-type define *bulk* rules that are part of a term but are neither the head nor the tail; the single D-type rule is equal to the sum over all the one-local terms in H . Using this categorization, each term in H should (a) either be formed from one C-type rule, one B-type rule, and any number of (possibly zero) A-type rules, or (b) be a one-body term included in the single D-type rule.

Once these rules are defined and categorized, it remains to resolve for the pre-factor of τ^n depending on how many terms in H appear in each term in \hat{O} . One solution is to modify the rules such that each term in H gains a factor τ . This can be achieved by multiplying either the C-type rule or the B-type rule by τ or, as shown in Table II, both rules by $\sqrt{\tau}$. This defines the two-dimensional generalization of the W^I approximation. At no increase of the number of signals required, the W^{II} approximation can be generated by considering products of terms who's support intersects only once. This manifests as allowing for products of rules that do not have any of the same signal non-zero. The background 0 signal essentially carries no information, and can be used to store the signals from the second operator in the product. If non-zero rules do overlap, then additional signals are needed (increasing the subsequent bond dimension of the tensor network operator) and are therefore ignored. The correct *second order* prefactor which can be determined from Table II, and the tensor network operator corresponding to the W^{II} approximation can be obtained from the FSA rules using Algorithm 1.

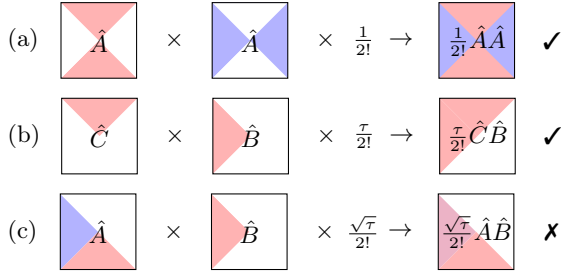


FIG. 3. (a) and (b) example of products of FSA rules that do not require additional levels, and can therefore be included at no cost to the operator bond dimension. In (c), the product includes overlapping non-trivial levels so we require an additional level to transmit both the blue and red signals simultaneously. Including such product rules allows the FSA to also generate all the second order terms that intersect only once.

1. Example: J_1 - J_2 Hamiltonian

It is useful to consider an example. Consider the following J_1 - J_2 Ising-like next-nearest neighbor Hamiltonian:

$$H_{\text{nnn}} = \left(J_1 \sum_{\langle j, k \rangle \in \Lambda} \hat{C}_j \hat{B}_k + J_2 \sum_{\langle\langle j, k \rangle\rangle \in \Lambda} \hat{C}_j \hat{B}_k + \text{h.c.} \right) + \sum_{j \in \Lambda} \hat{D}_j, \quad (8)$$

where the first sum is over the nearest-neighbors and the second sum is over the next-nearest neighbors (those directly diagonal to each other). We use h.c. as an abbreviation for the Hermitian conjugate of the written terms and make the choice $\hat{B} = \hat{C}^\dagger$ for all sites in the lattice.

The basic rules defining the FSA representation of this Hamiltonian are listed in Table I, *without* prefactors of τ . The resulting bond dimension of the tensor network operator is then, excluding the h.c. terms, $\eta_h = 3$ on the horizontal lattice direction, and $\eta_v = 2$, where the so-called unconventional path, indexed by 2, is not required. The total bond dimension including the h.c. terms is then $\eta_h = 5$ and $\eta_v = 3$. The un-conventional path is needed to prevent the FSA generating terms not in the Hamiltonian, as shown in Fig. 2. Note, this is not the only combination of rules capable of generating H_{nnn} . An alternative set of rules that lead to a symmetric tensor network operator for the common case of $\hat{C}_j \hat{B}_k = \hat{X}_j \hat{X}_k$ for all $j, k \in \Lambda$ is listed in Appendix B.

IV. LONG-RANGE INTERACTIONS

We now describe how long-range interactions can be represented in two-dimensions using FSA. By long-range we mean operators that act on arbitrary pairs of lattice sites at any distance from each other. Similar to the FSM construction for MPOs [54, 55, 72], the FSA construction

| Index (e, s, w, n) | Value | Rule type |
|--|------------------------------------|-----------|
| (0, 0, 0, 0) | $\mathbb{1}$ | identity |
| (0, 0, 0, 0) | $-i\hat{D}/k_{\max}$ | D |
| For all i and j in 1 to n_{\max} | | |
| ($i, 0, 0, 0$) | $-it_k \hat{C}$ | C |
| (0, 0, 0, i) | $-it_k \hat{C}$ | C |
| (0, 0, i , 0) | $s_{k,i} \lambda_{k,i} \hat{B}$ | B |
| (0, i , 0, 0) | $s_{k,i} \lambda_{k,i} \hat{B}$ | B |
| ($i, 0, i, 0$) | $\lambda_{k,i} \mathbb{1}$ | A |
| (0, $i, 0, i$) | $\lambda_{k,i} \mathbb{1}$ | A |
| ($i', 0, i', 0$) | $\lambda_{k,i} \mathbb{1}$ | A |
| ($j, i, 0, 0$) | $s_{k,j} \lambda_{k,j} \mathbb{1}$ | A |
| (0, $i, j', 0$) | $s_{k,j} \lambda_{k,j} \mathbb{1}$ | A |

TABLE III. Example of non-zero FSA rules that generate an approximation to a radial Gaussian function. The primed levels i' correspond to the so-called unconventional levels and should be given a distinct index to the unprimed level i . These rules should be used in combination with Table II and Algorithm 1.

allows us to represent Hamiltonians with long-range interactions by allowing the machine to remain on a given state indefinitely. Suppose we have a Hamiltonian H on a lattice Λ of the form

$$H = \left(\sum_{j \neq k \in \Lambda} V(x, y) \hat{C}_j \hat{B}_k + \text{h.c.} \right) + \sum_{j \in \Lambda} \hat{D}_j, \quad (9)$$

where x and y is the distance between the two lattice sites j and k along each respective lattice direction. In addition to rules for the J_1 - J_2 Hamiltonian listed in Table I, introducing the following A-type rules:

$$\square = \square = \square = \lambda \mathbb{1} \quad (10)$$

and also setting $J_2 J_1^{-1} = \lambda$ generates terms acting between lattice sites at all distances. The specific case of $\lambda = 1$ corresponds to all-to-all interactions, $V(x, y) = 1$, however this results in diverging interactions in the thermodynamic limit. The other limit $\lambda = 0$ is defines a model with completely localized interactions.

A. Gaussian approximation to the power law

When $|\lambda| < 0$, the strength of the interaction between two sites decays exponentially as a function of the Manhattan distance, $V(x, y) = \lambda^{|x|+|y|}$. Functions of the Euclidean distance $r = \sqrt{x^2 + y^2}$ can be constructed using a FSA by first approximating a Gaussian along each lattice direction as a finite sum of exponential functions [70], $e^{-\mu x^2} \approx g_\mu(x) = \sum_{k=1}^{n_k} s_k \lambda_k^x$, such that the FSA generates the product $g_\mu(x) g_\mu(y) \approx g_\mu(r)$. Then, defining a set of k_{\max} radial basis functions $f_k(x, y) =$

$g_{\mu_k}(x)g_{\mu_k}(y)$, the decay profile $V(x, y)$ can be approximated by the weighted sum $V(x, y) \approx \sum_{k=1}^{k_{\max}} t_k f_k(x, y)$ for $r = \sqrt{x^2 + y^2} > 0$. Note, for anisotropic lattices, one can have $g_{\mu_k}(x) \neq g_{\mu_k}(y)$ in general, however we only consider the simpler isotropic case.

1. Computing the optimal weights

The decay profile $V(x, y)$ is approximated by a function $f_{\text{fit}}(x, y)$ defined in terms of the parameters,

$$P_f = \{t_k, s_1, \dots, s_{n_k}, \lambda_1, \dots, \lambda_{n_k}\}_{k \in 1 \dots k_{\max}}. \quad (11)$$

we then wish to solve for P_f the optimization problem

$$\min_{P_f} \|V(x, y) - f_{\text{fit}}(x, y)\| \quad (12)$$

on the disc $D_{r_{\text{cut}}} = \{0 < \sqrt{x^2 + y^2} < r_{\text{cut}} \mid x, y \in \mathbb{Z}\}$, where r_{cut} is some finite radius cutoff. To do so, we use the algorithm described in Ref. [56] to compute the optimal expansion of the function $V(x, y)$ in terms of Gaussians. For $V(x, y) = r^\alpha$, we can directly apply the algorithm in Ref. [56] by finding the solution to (12) using $V(x, y) = r^{\alpha/2}$ in terms of exponentials λ_k^r and then subsequently taking $r \rightarrow r^2$ to find an approximation to r^α in terms of Gaussians $g_{\mu_k}(r) = e^{-\mu_k r^2}$. Then, assuming isotropy between the lattice directions, we again solve with $\mu_k = -\log \lambda_k$ where it is useful to allow for $s_k, \lambda_k \in \mathbb{C}$. Note, $g_{\mu_k}(r)$ only needs to be a good approximation of $e^{-\mu r^2}$ for $r \in \mathbb{Z}$ in contrast to f_{fit} where the elements of $D_{r_{\text{cut}}}$ are non-integer in general.

2. Quality of approximation

The parameters that control the quality of approximation are the number of Gaussian, k_{\max} that approximate the target function and, for each k , the number of exponential functions used to approximate each Gaussian $g_{\mu_k}(r)$ denoted $n_{k,\max}$. Depending on the value of μ_k , simply increasing $n_{k,\max}$ may not improve the approximation and may make it worse. As such, $n_{k,\max}$ is determined by choosing an integer n_{\max} such that $n_{k,\max} \leq n_{\max}$ and then selecting $n_{k,\max}$ that gives the best approximation for each k . An additional parameter g_{tol} defines the allowed tolerance in error $\epsilon_{\mu_k} = \sum_{r=1}^N |g_{\mu_k}(r) - e^{\mu_k r^2}|$ where an approximation with $n_{k,\max} < n_{\max}$ is selected. Any given value of g_{tol} then results in a non-unique combination of $n_{k,\max}$ for a given k_{\max} .

3. Time evolution operator

We can approximate the time evolution generated by the target Hamiltonian H given in (9) by first defining

$H^{[k]} = t_k \sum_{i,j \in \Lambda} f_k(x, y) \hat{C}_i \hat{B}_j + \sum_{i \in \Lambda} \hat{D}_i / k_{\max}$. We can now define the approximated fitting Hamiltonian H_{fit} as $H \approx H_{\text{fit}} = \sum_{k=1}^{k_{\max}} H^{(k)}$ provided $f_{\text{fit}}(x, y) \approx V(x, y)$. The Hamiltonian H_{fit} can then be represented as a FSA with $\mathcal{O}(k_{\max} n_{\max})$ non-trivial levels. This can be reduced to $\mathcal{O}(n_{\max})$ levels when constructing the time evolution operator by taking the Suzuki-Trotter decomposition [73, 74],

$$e^{\tau H_{\text{fit}}} = W^{[1]}(\tau) W^{[2]}(\tau) \dots W^{[k_{\max}]}(\tau) + \mathcal{O}(\tau^2), \quad (13)$$

where $W^{[k]}(\tau) = \exp(\tau H^{[k]})$, at the cost of k_{\max} update and truncation steps per time step. In terms of the size extensive cluster expansion (6), each $W^{[k]}(\tau)$ can then be represented by tensor network operator generated by the FSA rules listed in Table III each with bond dimension $\eta_h = 1 + 2n_{k,\max}$ along the horizontal direction and $\eta_v = 1 + n_{k,\max}$ along the vertical bonds where we do not requiring the additional level corresponding to the unconventional path. A vectorized Liouvillian super-operator representation would require (assuming one-local Lindblad operators) a real bond dimension of $\eta_k = (1 + 4n_{k,\max}, 1 + 2n_{k,\max})$ as one effectively has two entirely independent terms in the Hamiltonian, one from the ket space and one from the bra space.

One could in principle perform a Suzuki-Trotter decomposition over the terms appearing in $H^{(k)}$ that define the approximation to the Gaussian, however it was found that doing so resulted in instabilities caused by terms with very large interaction coefficient that would ordinarily cancel out when summed by the FSA.

V. APPLICATION TO LINDBLAD TIME EVOLUTION

We now describe how the operator construction just described can be applied to the case of Lindblad time evolution.

A. Tensor Network State Ansatz

We represent the density matrix on an infinite, two-dimensional square lattice as an iPEPO tensor network where each vertex $v \in \Lambda$ in the lattice is associated with a rank-6 tensor A_v with shape (d, d, D, D, D, D) . An edge between two vertices indicates a tensor contraction between the associated indices of the tensors at those vertices. The vectorization $|\rho\rangle\rangle$ is then obtained by fusing the physical index corresponding to the bra space with that of the ket space for all $\{A_v\}$, resulting in a network of rank-5 tensors with shape (d^2, D, D, D, D) functionally equivalent to an infinite projected entangled state operator (iPEPS). The tensor network structure is shown diagrammatically in Fig. 4a.

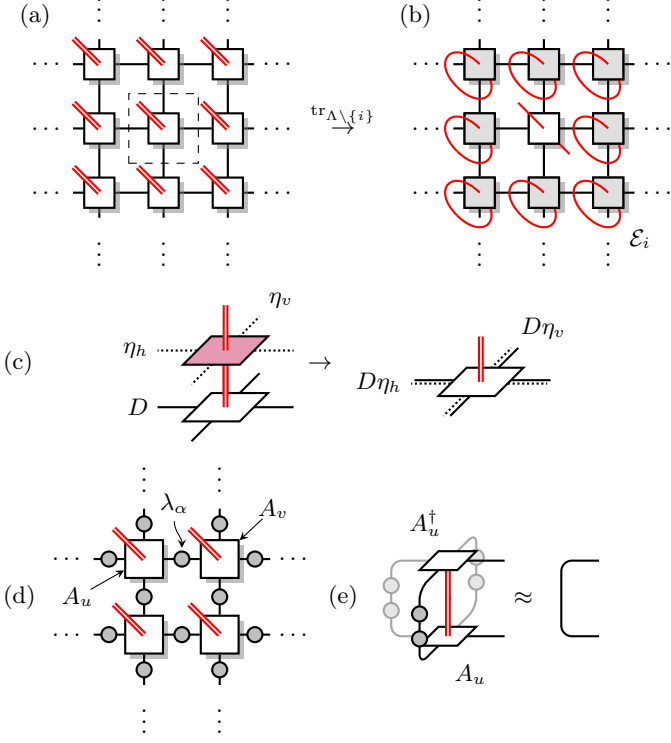


FIG. 4. (a) iPEPO parameterization of the vectorized state density matrix assuming a single-site unit-cell shown in the dashed box. The doubled red line denotes the physical bonds associated with each local vectorized Hilbert space $\mathcal{H}_v^\dagger \otimes \mathcal{H}_v$. (b) After un-vectorizing the state, local density matrices are obtained by computing the trace environment \mathcal{E}_i with respect to the i -th site in the lattice using an appropriate boundary algorithm as discussed in Appendix E. (c) Application of a tensor network super-operator to a single tensor of the vectorised iPEPO ansatz. (d) A state in the Vidal gauge has additional bond weights λ_α for each bond $\alpha = (u, v)$ in the lattice Λ . In the Vidal gauge, for each tensor A_u in the lattice, the quasi-orthogonality condition (e) is satisfied for all bonds incident to that tensor.

B. Vectorized Lindblad Equation

The Liouvillian super-operator is linear operator on the set of density matrices and can therefore be expressed as matrix of the form

$$\text{vec } \mathcal{L} = -i (\mathbb{1} \otimes H - H^\top \otimes \mathbb{1}) + \sum_k L_k^* \otimes L_k - \frac{1}{2} (\mathbb{1} \otimes L_k^\dagger L_k + L_k^\top L_k^* \otimes \mathbb{1}), \quad (14)$$

acting on the set of vectorized density matrices $|\rho\rangle\rangle$ defined previously. We then consider time-evolution generated by operators (14) that can be written in the form of (5), admitting a FSA representation, as described in Sec. III and Sec. IV. Further details of this construction can be found in Appendix C.

The density matrix is then evolved from a initial state at $t = 0$ to a state at time $t = n\Delta t$ via n repeated applications of the sequence of operators (13) (with $\tau := \Delta t$) to each tensor in the iPEPO as shown in Fig. 4c. In the limit $\Delta t \rightarrow 0$ both the Suzuki-Trotter approximation (13) and the extensive cluster expansion (6) become exact.

C. Bond truncation

After a single application of the tePEPO, all four bonds on each of the iPEPO tensors are simultaneously enlarged by a multiplicative factor of the tePEPO bond dimension η , i.e. $D \rightarrow D\eta$ (see Fig. 4c). To prevent the bond dimension growing exponentially, each bond is truncated back down to D using the simple-update (SU) method. SU requires putting the iPEPO in the Vidal gauge, where each bond hosts a matrix, known as the bond weight, which are used to construct a rank-1 approximation to the environment surrounding each bond [75]. When truncating the bond α from $D' > D$ back down to D , one replaces the $D' \times D'$ bond weight λ_α such that $\lambda_\alpha \rightarrow U \tilde{\lambda}_\alpha V^\dagger$, where $\tilde{\lambda}$ is a $D \times D$ matrix, and U_α and V_α are $D' \times D$ rectangular isometries. This truncates the dimension of the bond to D . How U_α and V_α are obtained is described in Appendix D.

During evolution with two-local Trotter gates, the Vidal gauge is implicitly maintained throughout the time-evolution, however this is not the case when applying tensor network operators in general, where more than one bond are updated simultaneously. To correctly perform simple update, the state must be re-gauged to re-obtain bond matrices on the composite bonds of size $D\eta$, which can be then truncated quasi-optimally by discarding the smallest elements of these, assuming the state is close enough to the Vidal gauge [76]. In doing so, it is assumed the rank-1 environment formed by the bond matrices accurately approximates the environment surrounding the bond being truncated, however this is uncontrolled.

In this work, we use a new variant of the simple update truncation method that avoids the need to re-gauge the enlarged network of $d^2 D^4 \eta^4$ -sized tensors, similar to the single-site version of the fast-full update method [77, 78] and the iterative truncation procedure described in Ref. [79]: after application of the tePEPO, immediately truncate all but a single bond in the network using the $D\eta \times D$ isometries U_α and V_α obtained for each bond from the previous timestep. The remaining bond is then truncated using the standard simple-update procedure, defining a new set of isometries and a new set of bond matrices for that particular bond. Using the following measure of convergence:

$$\delta^{[i]} < \max_{\alpha \in \Lambda} \|\lambda_\alpha^{[i]} - \lambda_\alpha^{[i-1]}\|, \quad (15)$$

where $\lambda_\alpha^{[i]}$ is the diagonal weight matrix on bond α after i -iterations, this process is iterated until $\delta^{[i]} < \epsilon_{\text{su}}$ where we have found $\epsilon_{\text{su}} = 1 \times 10^{-8}$ to be a useful convergence

threshold. This avoids the need to re-gauge the network before each truncation and reduces the complexity of the simple-update QR-decomposition from $\mathcal{O}(d^4 D^6 \eta^6)$ to $\mathcal{O}(d^4 D^6 \eta^3)$. We also found it useful for algorithm stability to fix the gauge of the iPEPO at the end of each time step. This is described in more detail in Appendix A.

D. Computing Observables

Observables can be obtained by first computing reduced density matrices with respect to a finite region of the infinite lattice. To do so, the scalar tensor network formed by contracting the physical indices of each tensor must be approximately contracted using a suitable boundary or tensor renormalization method. In this paper, the variational uniform matrix product state (VUMPS) method was used to find a boundary matrix product state (MPS) approximation to the upper and lower portions of the lattice around any given a row in combination with the left and right fixed points of the transfer matrices formed from the MPS and a single row of the lattice. Once these have been calculated, reduced density matrices of any size can be obtained by approximating the required partial trace of the infinite lattice with these boundary tensors, as shown in Appendix E.

VI. NUMERICAL RESULTS

A. Dissipative Long-Range Ising Model

As an initial technical benchmark of the method, we simulated the real time dynamics of the dissipative long-range transverse-field Ising model:

$$H = \frac{J}{\mathcal{N}(\alpha)} \sum_{j \neq k \in \Lambda} \frac{\hat{\sigma}_j^z \hat{\sigma}_k^z}{\|\mathbf{r}_j - \mathbf{r}_k\|^\alpha} + h \sum_{j \in \Lambda} \hat{\sigma}_j^x, \quad (16)$$

with dissipation occurring at a rate γ represented by the single onsite Lindblad operator $\hat{L}_j = \hat{\sigma}_j^z$. The parameter J defines the total strength of the interactions between lattice sites, and h the strength of the transverse field. The denominator $\mathcal{N}(\alpha)$ is the so-called Kac normalization [80] which for $\alpha > 2$ is finite with the analytical value $\mathcal{N}(\alpha) = 4\zeta(\alpha/2)\beta(\alpha/2)$ where $\zeta(x)$ and $\beta(x)$ are the Riemann zeta and Dirichlet beta functions respectively [53, 81]. This is used to rescale the *total* strength of the interactions on any given lattice site to be independent of α ensuring that any changes to the dynamics when changing α are caused by the change in the range of the interactions only. When $\alpha \leq 2$, $\mathcal{N}(\alpha)$ diverges and model is no longer well defined in the thermodynamic limit, so we do not consider that case here. As $\alpha \rightarrow \infty$, the short range model is recovered and $\mathcal{N}(\alpha \rightarrow \infty) = 4$ coinciding with the coordination number of the lattice.

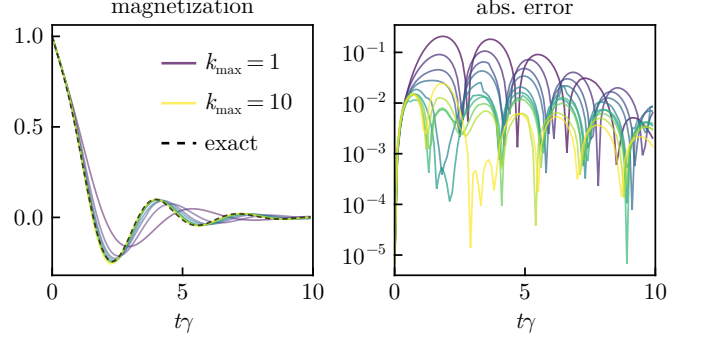


FIG. 5. Local magnetization along the x -axis $m^x = \langle \sigma_i^x \rangle$ of the long-range Ising model as a function of time for varying values of k_{\max} at bond dimension $D = 4$. The accuracy improves for increasing k_{\max} as shown in the inset where the absolute difference between the simulation and the exact solution (dashed) is plotted. The other hyper-parameters are $\text{max}_k n_k = 4$, $g_{\text{tol}} = 10^{-10}$ and $\Delta t = 0.01$.

1. Exactly solvable model

In the absence of any transverse field, $h = 0$, the Lindblad equation (1) with Hamiltonian (16) has an exact solution. We benchmark against this exact solution to assess how the FSA approximation to the power-law interaction effects the accuracy of the simulation. With $J/\gamma = 1.0$ and using an initial product state $\rho = \bigotimes |\uparrow_x\rangle\langle\uparrow_x|$, the model was simulated for a period of $t\gamma = 10$. The simulation was ran using a time step of $\Delta t = 0.01$ requiring a total of 1000 time steps, with truncations performed using itrSU with $\epsilon_{\text{su}} = 1 \times 10^{-8}$ and at most 20 iterations. In constructing the approximation, $g_{\text{tol}} = 1 \times 10^{-10}$.

First the effect of the cut-off k_{\max} in the power-law approximation is investigated by considering comparing with the exact solutions. As shown in Fig. 5, the accuracy of the simulation, with respect to the exact solution, improves for increasing k_{\max} , with low values $k_{\max} < 5$ leading to visually inaccurate results. For $k_{\max} = 10$, the results are similar to the exact solution with absolute error less than 1×10^{-2} for the majority of the time evolution. While, $k_{\max} = 10$ leads to the lowest absolute error during the late-time dynamics, defined here as $t\gamma \gtrsim 3.0$, before this, where the magnetization changes most rapidly, more accurate results can be achieved with smaller values of k_{\max} . This is likely a consequence larger k_{\max} requiring more Trotter steps and thus more truncations which may not be found optimally via the uncontrolled simple update approximation. This is supported by an increased entanglement during this period as evidenced by the peak in bond entropy plotted in Fig. 6.

We also investigated how the simulation performs when reducing the dissipation, equivalent to increasing the interaction strength. It is expected that as the dissipation decreases, the entanglement will increase at a faster rate, compromising the accuracy of the finite bond-dimension tensor network simulation at early times [44].

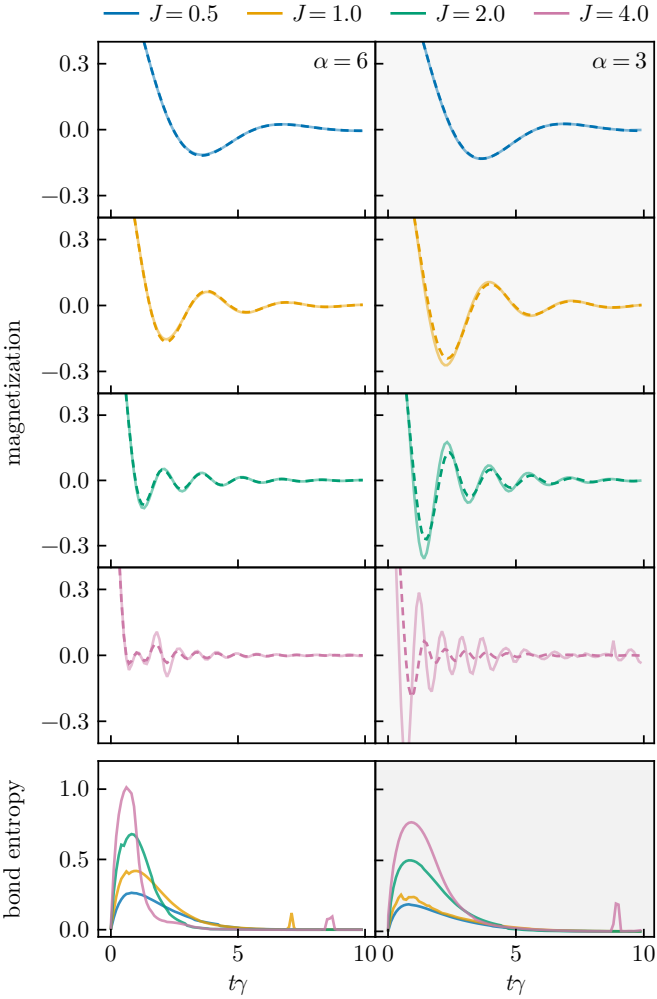


FIG. 6. Comparison between the van der Waals case, $\alpha = 6$, (left, white background) and the dipolar case, $\alpha = 3$, (right, gray, background) of the long-range dissipative Ising model (16) at varying interaction strength J . The bond entropy (two bottom panels) is larger for increasing J , which is associated with worsening accuracy. The dissipation is set to $\gamma = 1$. All other parameters are the same as in Fig. 5.

To estimate this amount of entanglement in the system, we use the bond entropy,

$$S_\alpha = - \sum_{j=1}^D [\lambda_\alpha]_{jj} \log [\lambda_\alpha]_{jj}, \quad (17)$$

which acts as a proxy to the true entanglement. For acyclic tensor networks, the quantity S_α defined in (17) reduces to the true entanglement entropy between the two regions of the network defined by cutting the bond α .

Fixing $k_{\max} = 20$ and $n_{\max} = 4$, Fig. 6 plots the magnetization for a range of interaction strengths $J/\gamma \in \{0.5, 1.0, 2.0, 4.0\}$. The bottom panels of Fig. 6 show the peak in the bond entropy at a higher value for increasing J/γ , where the simulated dynamics tends to deviate

the most from the exact solution. Interestingly, the less-accurate $\alpha = 3$ simulations are associated with a shorter but broader peak in bond entropy suggesting that more prolonged periods of high bond entropy are more problematic than those with sharp but brief peaks.

2. Beyond exactly solvable regime

To assess the performance of the method in a regime not yet amenable to an exact solution, the model (16) is simulated with transverse magnetic field of strength $h/\gamma = 0.5$. In this case, there is no known exact solution to the model (16). Compared to the exactly solvable case, the solution appears to move toward a non-trivial steady-state with non-zero bond entropy, non-zero correlations and finite magnetization; the results are shown in Fig. 7. When $J/\gamma = 0.5$, the long time dynamics are effected by the bond dimension most significantly, with results $D \geq 8$ visually agreeing with each other, but visually distinct from the simulations with $D = 6$ and $D = 7$. This can be seen in panels (a.i–a.iv) in Fig. 7. The time dynamics are smoothest for bond dimension $D = 10$ in all panels, however good convergence is found for lower bond dimension $D < 10$ for the case of $J/\gamma = 1.0$. For the case $J/\gamma = 2.0$, the time dynamics are more difficult to converge with respect to the bond dimension, with some unstable regions in time for $D \in \{6, 7\}$, however simulations with $D = 10$ are smooth for all computed quantities. This demonstrates that the method is applicable to models with long-range interactions beyond the exactly solvable regime, provided care is taken to ensure convergence with bond dimension.

B. Rydberg Hamiltonian

Finally, we consider a physically-motivated example. The long-range Ising model can be realized experimentally using an array of atoms that can in either an excited Rydberg state $|r\rangle$ or a ground state $|g\rangle$. When excited, each atom creates a strong short-range repulsive potential that is typically of van der Waals type r^{-6} . However, for certain species of Rydberg atoms, the underlying r^{-3} dipole-dipole interaction can be recovered via an effect known as Förster resonance [82], leading to a dipole-dipole blockading effect useful for quantum information processing [83]. Including a laser driving field and local dissipation from the excited state to ground state [53], we consider the following model Hamiltonian:

$$H = \frac{V}{\mathcal{N}(\alpha)} \sum_{j \neq k \in \Lambda} \frac{\hat{n}_j \hat{n}_k}{\|\mathbf{r}_j - \mathbf{r}_k\|^\alpha} - \frac{\Omega}{2} \sum_{j \in \Lambda} \hat{\sigma}_j^x + \Delta \sum_{j \in \Lambda} \hat{n}_j \quad (18)$$

together with Lindblad operator $L_j = \sqrt{\gamma} |g_j\rangle \langle r_j|$ evolving according to the Lindblad equation (1), where $\hat{n}_j = |r_j\rangle \langle r_j|$ and $\hat{\sigma}_j^x = |g_j\rangle \langle r_j| + |r_j\rangle \langle g_j|$. The parameter $V/\mathcal{N}(\alpha)$ represents the Kac-normalized repul-

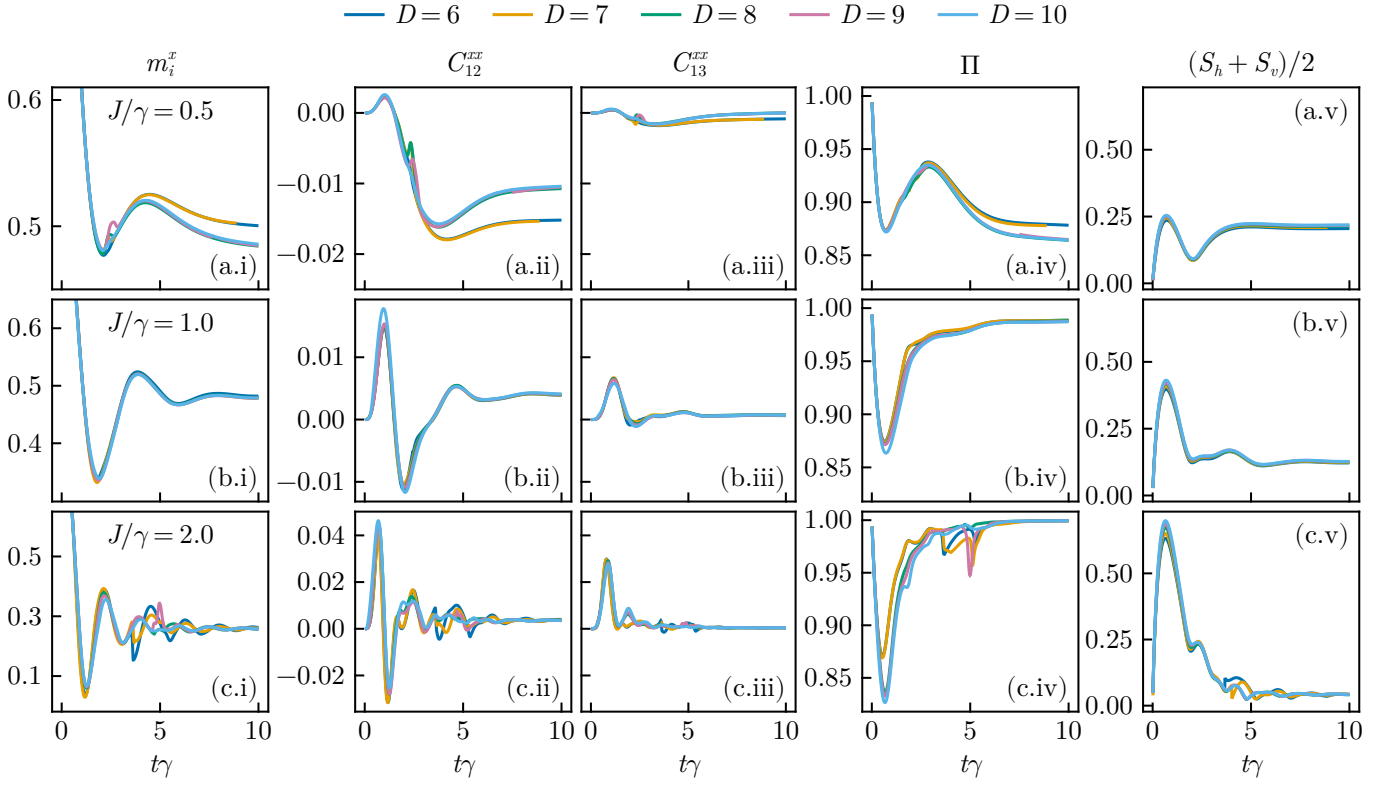


FIG. 7. Plots of (i) magnetization $m_i^x = \langle \hat{\sigma}_i^x \rangle$, correlators (ii) C_{12}^{xx} and (iii) C_{13}^{xx} where $C_{ij}^{xx} = \langle \hat{\sigma}_i^x \hat{\sigma}_j^x \rangle - \langle \hat{\sigma}_i^x \rangle \langle \hat{\sigma}_j^x \rangle$, (iv) purity, and (v) bond entropy of the long-range transverse field Ising model with $\alpha = 3.0$, $h/\gamma = 0.5$ and J/γ equal to (a) 0.5, (b) 1.0 (c) 2.0. A time step of $\Delta t = 1.25 \times 10^{-2}$ was used and bonds were truncated using parallel itrSU with a tolerance of 1×10^{-8} . In constructing the approximation to the power law, $k_{\max} = 10$ Gaussians were used with $g_{\text{tol}} = 1 \times 10^{-5}$ and $n_{\max} = 4$.

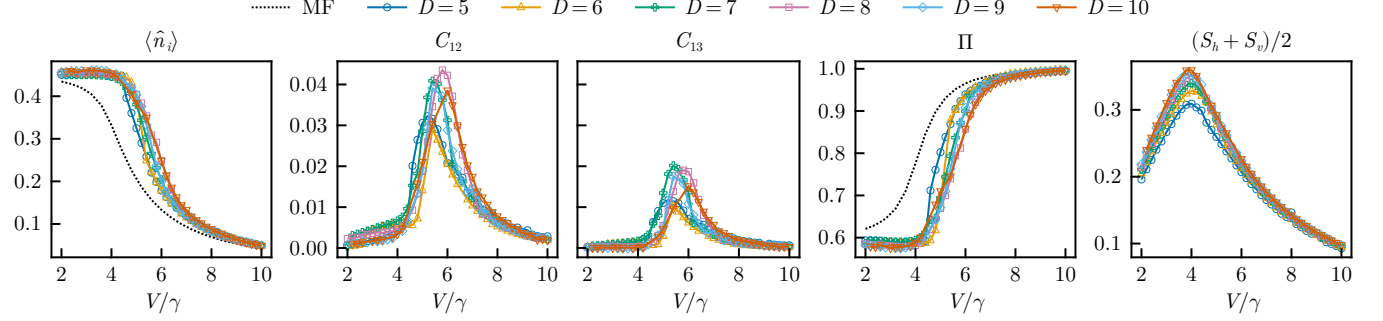


FIG. 8. Steady state of the Rydberg Hamiltonian (18) with $\Omega/\gamma = 2.0$ and $\Delta = -V/2\gamma$ at bond dimension $D \in 5..10$. The mean-field (dashed line) is plotted for observables where this is non-trivial. From left to right: the average occupation $\langle \hat{n}_i \rangle$, nearest-neighbor and next-nearest neighbor correlations $C_{jk} = \langle \hat{n}_j \hat{n}_k \rangle - \langle \hat{n}_j \rangle \langle \hat{n}_k \rangle$, average purity Π , and the bond entropy $(S_h + S_v)/2$.

sion strength, Ω the Rabi frequency, Δ the laser detuning, and γ the dissipation rate. Variants of this model have been studied on a one-dimensional lattice with tree-tensor networks [39], however that particular ansatz is unable to capture area-law when applied to two-dimensional systems in general, and via a variational Monte Carlo applied to a matrix-product state ansatz [23]. In two-dimensions, the steady-state of the van der Waals case, $\alpha = 6$, has been studied using variational methods [53], and in higher-dimensions using a

semi-classical phase-space approach [28].

1. Steady state

In Fig. 8 we plot the steady state at bond dimensions in the interval $D \in 5..10$. A time step of $\Delta t = 1.25 \times 10^{-2}$ was used, and the simulation was ran for 2000 iterations. The parallel version of iterative simple update method was used to truncate the bonds after the application of

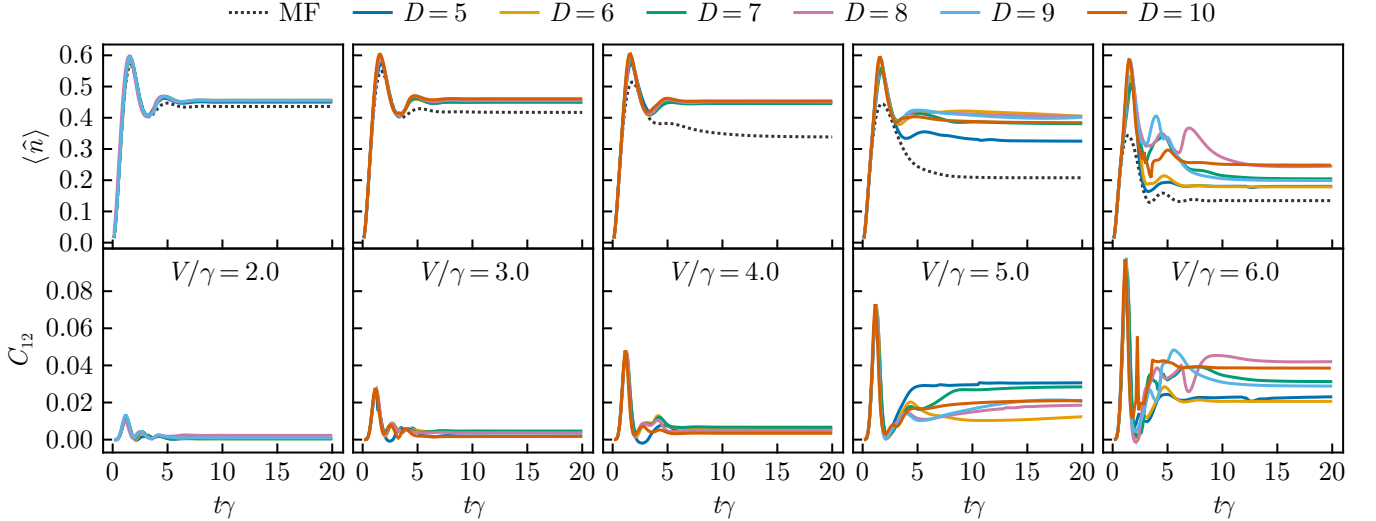


FIG. 9. Time dynamics of the Rydberg Hamiltonian (18) with $\Omega/\gamma = 2.0$ and $\Delta = -V/2\gamma$ at bond dimension $D \in 5 \dots 10$. The mean-field solution (dashed line) is plotted along side for observables where this is non-trivial.

each tePEPO operator.

We observe crossover from a phase with high average population $\langle \hat{n}_j \rangle$ to a phase with low average population as the strength of the interactions increase, characteristic of the dipole-dipole blockading effect. This crossover occurs at $V/\gamma \approx 6.0$ where there is also an increase in the correlations $C_{jk} = \langle \hat{n}_j \hat{n}_k \rangle - \langle \hat{n}_j \rangle \langle \hat{n}_k \rangle$ between nearest-neighbor and next-nearest-neighbor sites (C_{12} and C_{13} respectively) in the lattice. There is also associated with a transition from a mixed state with purity $\Pi \approx 0.6$ to a pure state with $\Pi \rightarrow 1.0$ as the dissipation rate γ is decreased. At large V/γ the steady state becomes pure and one again well approximated by the mean field solution.

The sum of the bond entropy on each bond ($S_h + S_v$)/2 appears to peak at $V/\gamma \approx 4.0$ where the simulated result begins to deviate most significantly from the mean-field solution. This is expected considering the limit of zero bond entropy resulting from a product state with all bond weights having only a single non-zero singular value.

2. Dynamics

In Figure 9, the real time dynamics at low-to-moderate interaction strength $V/\gamma \in \{2.0, 3.0, 4.0, 5.0, 6.0\}$, is plotted. Stable time-evolution is achieved when $V/\gamma \leq 5.0$ showing significant corrections to the mean field solution, also plotted. At $V\gamma = 6.0$, the time dynamics begin to deteriorate as the crossover point is traversed. Near this crossover point, the simulation deviates from the mean-field significantly and there is an associated increase in the correlations between neighboring lattice sites.

At high interaction strength, $V\gamma \in \{8.0, 10.0\}$, the rapid dynamics in the initial stages of the time evolution $t\gamma < 5.0$ leads to poor convergence of the trace environment for larger V/γ leading to unreliable results during

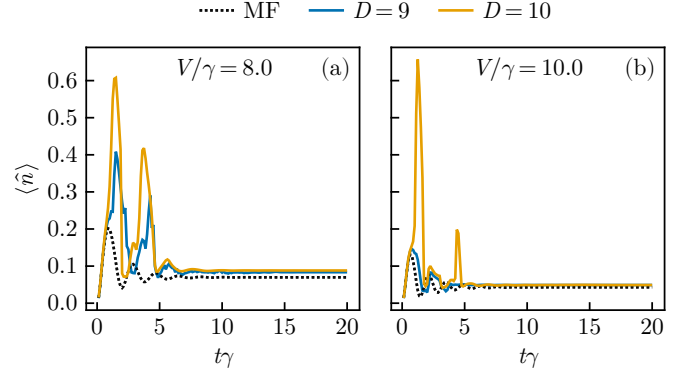


FIG. 10. Dynamics of the Rydberg Hamiltonian (18) in the weakly dissipative regime simulated using the tePEPO method at bond dimension $D = 9$ and $D = 10$. While dynamics are unstable at short times, convergence to a steady state at later times is not compromised.

this time period. This is shown in by the larger imaginary part of the average occupation, shown in Figure 10. However, we still find smooth evolution for at late time, and the initial unstable time evolution at $t < 5.0$ does not appear to compromise the simulation at later times; the simulation stabilizes and convergence to a steady state is still achieved.

3. Comparison with short-range model

A corresponding short-range (nearest-neighbor) model can be recovered in the limit $\alpha \rightarrow \infty$. In this limit, we found that simulations with existing tensor network methods [43] fail to converge to a steady state and can be unstable in the worst case, with possibly spurious limit cycles emerging for certain simulation parameters. The

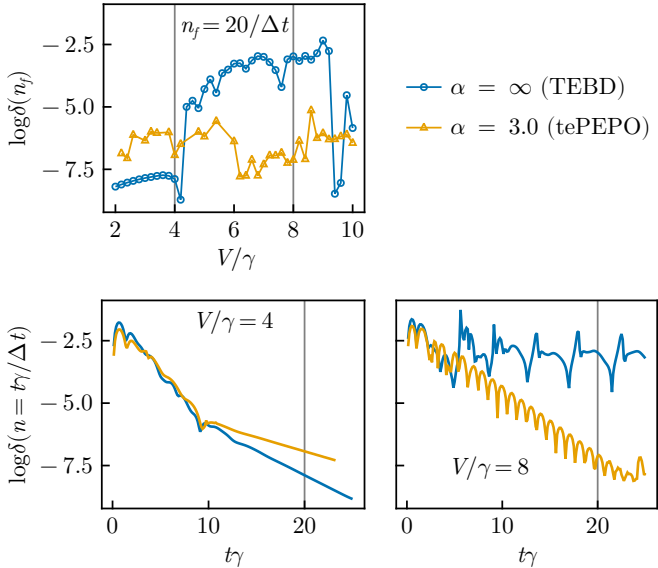


FIG. 11. Steady state convergence at $D = 10$ using $\tau = 1.25 \times 10^{-2}$ for the tePEPO method compared to the short range model ($\alpha \rightarrow \infty$) simulated with TEBD. For the short range model, convergence cannot be achieved for much of the region $V/\gamma > 4$, whereas the simulation of $\alpha = 3.0$ using tePEPO are able to converge in this regime. For $V/\gamma \leq 4$, both cases converge.

tePEPO method of this work is not expected to perform any better in this case, however it allows for simulation of the long-range regime beyond nearest-neighbor $2 < \alpha < \infty$. This is in contrast to the short-range model, simulated using TEBD and standard simple update, where no steady state is achieved; by increasing the range of the interactions from short-range to dipolar, the time dynamics become more stable and convergence to steady states can be achieved for a much wider range of interaction strength V/γ .

To measure convergence in time, we use the quantity $\delta^{[n]}$ defined in (15) rescaled according to the time step $\delta^{[n]} \rightarrow \delta^{[n]}/\Delta t$, with n referring to the n -th time step of the simulation such that $t = n\Delta t$. As shown in Fig. 11, the short range model typical fails to converge in time when $V/\gamma > 1.0$. On the other hand, the long-range model ($\alpha = 3.0$) solved with the tePEPO method converges similarly for all values of V/γ despite worse convergence in parameter regions where convergence can be found in the short range model. This suggests the existence of long-range Lindblad equations that are amenable to simulations with tensor networks despite the corresponding short-range model failing to converge.

VII. DISCUSSION

We have proposed a construction of tensor network operators able to simulate the real and imaginary time dynamics of two-dimensional quantum lattice system, and

have benchmarked the method against the extreme example of systems with power-law long-range interactions, where we described how such interaction profiles can be approximated as sums of simpler terms. We show that only a modest number of terms in this sum are required for visibly accurate results. Our new simple-update based iterative truncation method is capable of efficient bond truncations when evolving using tensor network operators.

As with most high-dimensional tensor network methods, the core computational bottleneck remains the bond truncation step. Despite it's efficiency, itrSU lacks the robustness of the regular simple update method, while still relying on a good approximation to the Vidal gauge being achievable, which may not always be the case. Furthermore, itrSU assumes the same uncontrolled approximation to the environment. We found that the correlation length ξ was on the order of a few lattice sites $\xi \gtrsim 2$, suggesting that correlations extend beyond that which can be captured by bond weights in the simple update method. Therefore, the *environment* update, such as the fast full update [77–79], will potentially improve the stability and accuracy of our method in these regions, where the correlation length becomes larger. Another extension could be to truncate using the recently developed belief propagation method [75], where the usually uncontrolled simple update approximation can be systematically improved by including loop corrections [84].

The large class of Hamiltonians (and indeed Lindblad operators) that permit time evolution operators in terms of FSA remains largely unexplored. The extension to beyond on-site dissipation is straightforward, and would simply involve writing the three terms appearing in the vectorization of each Lindblad operator as FSA rules, as shown in Appendix C. Non-trivial dissipation has been associated with a wide range of quantum phenomena such as quantum time crystals [85], and quantum state preparation [5], to name a few. Finally, the examples presented in this paper are two-level many-body systems. The extension to larger local Hilbert spaces is trivial and to fermions is also in principle straightforward. In the former one has the advantage that the bond dimension of the operator is decoupled from dimension of the local Hilbert space. The path structure of the FSA also allows encoding mediated cluster operators, such as those obtained from the Jordan-Wigner transformation, at no extra cost to the operator bond dimension. In summary, this work represents a major advancement in simulating the dynamics of higher-dimensional quantum systems with tensor networks, and opens up new avenues in the study of novel many-body phenomena in both open and finite temperature quantum systems, as well as realistic quantum devices.

Acknowledgments. The authors thank Dawid Hynriuk for valuable discussions and feedback on the manuscript. This work was supported by the Engineering and Physical Sciences Research Council [grant number EP/S021582/1], and the European Union under Horizon

Europe (project No. 101186579). The authors acknowledge the use of the UCL HPC facilities and associated support services in the completion of this work.

DATA AVAILABILITY

The data that support the findings of this article are openly available [86].

[1] M. Schlosshauer, Quantum decoherence, *Physics Reports Quantum Decoherence*, **831**, 1 (2019).

[2] F. Verstraete, M. M. Wolf, and J. I. Cirac, Quantum computation and quantum-state engineering driven by dissipation, *Nat. Phys.* **5**, 633 (2009).

[3] D. C. Cole, J. J. Wu, S. D. Erickson, P.-Y. Hou, A. C. Wilson, D. Leibfried, and F. Reiter, Dissipative preparation of W states in trapped ion systems, *New J. Phys.* **23**, 073001 (2021).

[4] F. Yang, P. Molignini, and E. J. Bergholtz, Dissipative boundary state preparation, *Phys. Rev. Res.* **5**, 043229 (2023).

[5] M. Wampler and N. R. Cooper, *Absorbing State Phase Transitions and Stability of Long-Range Coherence in Dissipative Quantum State Preparation* (2024), arXiv:2410.00819.

[6] Y. Zhan, Z. Ding, J. Huhn, J. Gray, J. Preskill, G. K.-L. Chan, and L. Lin, *Rapid quantum ground state preparation via dissipative dynamics* (2025), arXiv:2503.15827 [quant-ph].

[7] J. M. Gertler, B. Baker, J. Li, S. Shirol, J. Koch, and C. Wang, Protecting a bosonic qubit with autonomous quantum error correction, *Nature* **590**, 243 (2021).

[8] J. Carrasco, J. R. Maze, C. Hermann-Avigliano, and F. Barra, Collective enhancement in dissipative quantum batteries, *Phys. Rev. E* **105**, 064119 (2022).

[9] A. Amo and J. Bloch, Exciton-polaritons in lattices: A non-linear photonic simulator, *C. R. Phys.* **17**, 934 (2016).

[10] F. Schäfer, T. Fukuvara, S. Sugawa, Y. Takasu, and Y. Takahashi, Tools for quantum simulation with ultracold atoms in optical lattices, *Nat Rev Phys* **2**, 411 (2020).

[11] A. Blais, A. L. Grimsmo, S. M. Girvin, and A. Wallraff, Circuit quantum electrodynamics, *Reviews of Modern Physics* **93**, 025005 (2021).

[12] H. Walther, B. T. H. Varcoe, B.-G. Englert, and T. Becker, Cavity quantum electrodynamics, *Reports on Progress in Physics* **69**, 1325 (2006).

[13] M. Foss-Feig, J. T. Young, V. V. Albert, A. V. Gorshkov, and M. F. Maghrebi, Solvable Family of Driven-Dissipative Many-Body Systems, *Phys. Rev. Lett.* **119**, 190402 (2017).

[14] A. McDonald and A. A. Clerk, Exact Solutions of Interacting Dissipative Systems via Weak Symmetries, *Phys. Rev. Lett.* **128**, 033602 (2022).

[15] L. M. Sieberer, M. Buchhold, and S. Diehl, Keldysh field theory for driven open quantum systems, *Rep. Prog. Phys.* **79**, 096001 (2016).

[16] M. F. Maghrebi and A. V. Gorshkov, Nonequilibrium many-body steady states via Keldysh formalism, *Physical Review B* **93**, 014307 (2016).

[17] A. Nagy and V. Savona, Driven-dissipative quantum Monte Carlo method for open quantum systems, *Physical Review A* **97**, 052129 (2018).

[18] M. J. Hartmann and G. Carleo, Neural-Network Approach to Dissipative Quantum Many-Body Dynamics, *Phys. Rev. Lett.* **122**, 250502 (2019).

[19] A. Nagy and V. Savona, Variational Quantum Monte Carlo Method with a Neural-Network Ansatz for Open Quantum Systems, *Phys. Rev. Lett.* **122**, 250501 (2019).

[20] F. Vicentini, A. Biella, N. Regnault, and C. Ciuti, Variational Neural-Network Ansatz for Steady States in Open Quantum Systems, *Phys. Rev. Lett.* **122**, 250503 (2019).

[21] N. Yoshioka and R. Hamazaki, Constructing neural stationary states for open quantum many-body systems, *Phys. Rev. B* **99**, 214306 (2019).

[22] S. Kothe and P. Kirton, Liouville-space neural network representation of density matrices, *Physical Review A* **109**, 062215 (2024).

[23] D. A. Hryniuk and M. H. Szymańska, Tensor-network-based variational Monte Carlo approach to the non-equilibrium steady state of open quantum systems, *Quantum* **8**, 1475 (2024).

[24] D. A. Hryniuk and M. H. Szymańska, *Variational approach to open quantum systems with long-range competing interactions* (2025), arXiv:2510.01543 [quant-ph].

[25] M. Troyer and U.-J. Wiese, Computational Complexity and Fundamental Limitations to Fermionic Quantum Monte Carlo Simulations, *Phys. Rev. Lett.* **94**, 170201 (2005).

[26] C. D. Mink, D. Petrosyan, and M. Fleischhauer, Hybrid discrete-continuous truncated Wigner approximation for driven, dissipative spin systems, *Phys. Rev. Res.* **4**, 043136 (2022).

[27] V. P. Singh and H. Weimer, Driven-Dissipative Criticality within the Discrete Truncated Wigner Approximation, *Phys. Rev. Lett.* **128**, 200602 (2022).

[28] J. Huber, A. M. Rey, and P. Rabl, Realistic simulations of spin squeezing and cooperative coupling effects in large ensembles of interacting two-level systems, *Phys. Rev. A* **105**, 013716 (2022).

[29] M. Van Regemortel, W. Casteels, I. Carusotto, and M. Wouters, Spontaneous Beliaev-Landau scattering out of equilibrium, *Phys. Rev. A* **96**, 053854 (2017).

[30] P. Deuar, A. Ferrier, M. Matuszewski, G. Orso, and M. H. Szymańska, Fully Quantum Scalable Description of Driven-Dissipative Lattice Models, *PRX Quantum* **2**, 010319 (2021).

[31] S. R. White, Density-matrix algorithms for quantum renormalization groups, *Physical Review B* **48**, 10345 (1993).

[32] U. Schollwöck, The density-matrix renormalization group in the age of matrix product states, *Annals of Physics January 2011 Special Issue*, **326**, 96 (2011).

[33] F. Verstraete, J. J. García-Ripoll, and J. I. Cirac, Matrix Product Density Operators: Simulation of Finite-Temperature and Dissipative Systems, *Physical Review Letters* **93**, 207204 (2004).

[34] J. Cui, J. I. Cirac, and M. C. Bañuls, Variational Matrix Product Operators for the Steady State of Dissipative Quantum Systems, *Physical Review Letters* **114**, 220601 (2015).

[35] E. Mascarenhas, H. Flayac, and V. Savona, Matrix-product-operator approach to the nonequilibrium steady state of driven-dissipative quantum arrays, *Physical Review A* **92**, 022116 (2015).

[36] A. H. Werner, D. Jaschke, P. Silvi, M. Kliesch, T. Calarco, J. Eisert, and S. Montangero, Positive Tensor Network Approach for Simulating Open Quantum Many-Body Systems, *Physical Review Letters* **116**, 237201 (2016).

[37] A. A. Gangat, T. I, and Y.-J. Kao, Steady States of Infinite-Size Dissipative Quantum Chains via Imaginary Time Evolution, *Physical Review Letters* **119**, 010501 (2017).

[38] See D. Jaschke, S. Montangero, and L. D. Carr, One-dimensional many-body entangled open quantum systems with tensor network methods, *Quantum Sci. Technol.* **4**, 013001 (2018) for an example of how to construct the required MPO form of a Liouvillian.

[39] D. Sulz, C. Lubich, G. Ceruti, I. Lesanovsky, and F. Carollo, Numerical simulation of long-range open quantum many-body dynamics with tree tensor networks, *Phys. Rev. A* **109**, 022420 (2024).

[40] E. Godinez-Ramirez, R. Milbradt, and C. B. Mendl, *A Riemannian Approach to the Lindbladian Dynamics of a Locally Purified Tensor Network* (2024), arXiv:2409.08127.

[41] J. Saiphet and D. Braun, Simulation of the dissipative dynamics of strongly interacting nitrogen-vacancy centers with tensor networks, *Phys. Rev. A* **111**, 022604 (2025).

[42] J. Allen, M. Otten, S. Gray, and B. K. Clark, *Simulating Neutral Atom Quantum Systems with Tensor Network States* (2025), arXiv:2309.08572 [quant-ph].

[43] A. Kshetrimayum, H. Weimer, and R. Orús, A simple tensor network algorithm for two-dimensional steady states, *Nat Commun* **8**, 1291 (2017).

[44] C. M. Keever and M. H. Szymańska, Stable iPEPO tensor-network algorithm for dynamics of two-dimensional open quantum lattice models, *Phys. Rev. X* **11**, 021035 (2021).

[45] D. Kilda, A. Biella, M. Schiro, R. Fazio, and J. Keeling, On the stability of the infinite Projected Entangled Pair Operator ansatz for driven-dissipative 2D lattices, *SciPost Phys. Core* **4**, 5 (2021).

[46] G. Vidal, Efficient Simulation of One-Dimensional Quantum Many-Body Systems, *Physical Review Letters* **93**, 040502 (2004).

[47] S. R. White and A. E. Feiguin, Real-Time Evolution Using the Density Matrix Renormalization Group, *Physical Review Letters* **93**, 076401 (2004).

[48] A. J. Daley, C. Kollath, U. Schollwöck, and G. Vidal, Time-dependent density-matrix renormalization-group using adaptive effective Hilbert spaces, *Journal of Statistical Mechanics: Theory and Experiment* **2004**, P04005 (2004).

[49] J. Haferkamp, D. Hangleiter, J. Eisert, and M. Gluza, Contracting projected entangled pair states is average-case hard, *Physical Review Research* **2**, 013010 (2020).

[50] M. Raghunandan, J. Wrachtrup, and H. Weimer, High-Density Quantum Sensing with Dissipative First Order Transitions, *Phys. Rev. Lett.* **120**, 150501 (2018).

[51] H. Bernien, S. Schwartz, A. Keesling, H. Levine, A. Omran, H. Pichler, S. Choi, A. S. Zibrov, M. Endres, M. Greiner, V. Vuletić, and M. D. Lukin, Probing many-body dynamics on a 51-atom quantum simulator, *Nature* **551**, 579 (2017).

[52] S. Ebadi, T. T. Wang, H. Levine, A. Keesling, G. Semeghini, A. Omran, D. Bluvstein, R. Samajdar, H. Pichler, W. W. Ho, S. Choi, S. Sachdev, M. Greiner, V. Vuletić, and M. D. Lukin, Quantum phases of matter on a 256-atom programmable quantum simulator, *Nature* **595**, 227 (2021).

[53] J. Kazemi and H. Weimer, Driven-Dissipative Rydberg Blockade in Optical Lattices, *Phys. Rev. Lett.* **130**, 163601 (2023).

[54] M. P. Zaletel, R. S. K. Mong, C. Karrasch, J. E. Moore, and F. Pollmann, Time-evolving a matrix product state with long-ranged interactions, *Phys. Rev. B* **91**, 165112 (2015).

[55] M. Van Damme, J. Haegeman, I. McCulloch, and L. Vanderstraeten, Efficient higher-order matrix product operators for time evolution, *SciPost Physics* **17**, 135 (2024).

[56] B. Pirvu, V. Murg, J. I. Cirac, and F. Verstraete, Matrix product operator representations, *New Journal of Physics* **12**, 025012 (2010).

[57] H.-P. Breuer and F. Petruccione, *The Theory of Open Quantum Systems* (Oxford University Press, 2007).

[58] G. M. Crosswhite and D. Bacon, Finite automata for caching in matrix product algorithms, *Phys. Rev. A* **78**, 012356 (2008).

[59] B. Vanhecke, L. Vanderstraeten, and F. Verstraete, Symmetric cluster expansions with tensor networks, *Phys. Rev. A* **103**, L020402 (2021).

[60] D. E. Parker, X. Cao, and M. P. Zaletel, Local matrix product operators: Canonical form, compression, and control theory, *Phys. Rev. B* **102**, 035147 (2020).

[61] M. E. Fisher and W. Selke, Infinitely Many Commensurate Phases in a Simple Ising Model, *Phys. Rev. Lett.* **44**, 1502 (1980).

[62] W. Selke, The ANNNI model — Theoretical analysis and experimental application, *Physics Reports* **170**, 213 (1988).

[63] T. Eckstein, R. Mansuroglu, P. Czarnik, J.-X. Zhu, M. J. Hartmann, L. Cincio, A. T. Sornborger, and Z. Holmes, Large-scale simulations of Floquet physics on near-term quantum computers, *npj Quantum Inf* **10**, 1 (2024).

[64] N. Defenu, A. Trombettoni, and S. Ruffo, Anisotropic long-range spin systems, *Phys. Rev. B* **94**, 224411 (2016).

[65] P. Corboz, G. Evenbly, F. Verstraete, and G. Vidal, Simulation of interacting fermions with entanglement renormalization, *Phys. Rev. A* **81**, 010303 (2010).

[66] O. Gauthé and F. Mila, Thermal Ising Transition in the Spin-\$1/2\\$ \$\{J\}_1\\$-\\$J\}_2\\$ Heisenberg Model, *Phys. Rev. Lett.* **128**, 227202 (2022).

[67] O. Gauthé and F. Mila, Thermal Phase Diagram of the Square Lattice Ferro-antiferromagnetic J_1 - J_2 Heisenberg Model (2023), [arXiv:2310.09344](https://arxiv.org/abs/2310.09344).

[68] M. J. O'Rourke, Z. Li, and G. K.-L. Chan, Efficient representation of long-range interactions in tensor network algorithms, *Phys. Rev. B* **98**, 205127 (2018).

[69] Z. Li, M. J. O'Rourke, and G. K.-L. Chan, Generalization of the exponential basis for tensor network representations of long-range interactions in two and three dimensions, *Phys. Rev. B* **100**, 155121 (2019).

[70] M. J. O'Rourke and G. K.-L. Chan, Simplified and improved approach to tensor network operators in two dimensions, *Phys. Rev. B* **101**, 205142 (2020).

[71] M. J. O'Rourke and G. K.-L. Chan, Entanglement in the quantum phases of an unfrustrated Rydberg atom array, *Nat Commun* **14**, 5397 (2023).

[72] G. M. Crosswhite, A. C. Doherty, and G. Vidal, Applying matrix product operators to model systems with long-range interactions, *Phys. Rev. B* **78**, 035116 (2008).

[73] H. F. Trotter, On the product of semi-groups of operators, *Proc. Amer. Math. Soc.* **10**, 545 (1959).

[74] M. Suzuki, Generalized Trotter's formula and systematic approximants of exponential operators and inner derivations with applications to many-body problems, *Commun. Math. Phys.* **51**, 183 (1976).

[75] J. Tindall and M. Fishman, Gauging tensor networks with belief propagation, *SciPost Physics* **15**, 222 (2023).

[76] H. Kalis, D. Klagges, R. Orús, and K. P. Schmidt, Fate of the cluster state on the square lattice in a magnetic field, *Phys. Rev. A* **86**, 022317 (2012).

[77] H. N. Phien, I. P. McCulloch, and G. Vidal, Fast convergence of imaginary time evolution tensor network algorithms by recycling the environment, *Phys. Rev. B* **91**, 115137 (2015).

[78] H. N. Phien, J. A. Bengua, H. D. Tuan, P. Corboz, and R. Orús, Infinite projected entangled pair states algorithm improved: Fast full update and gauge fixing, *Phys. Rev. B* **92**, 035142 (2015).

[79] P. Czarnik and J. Dziarmaga, Projected entangled pair states at finite temperature: Iterative self-consistent bond renormalization for exact imaginary time evolution, *Phys. Rev. B* **92**, 035120 (2015).

[80] M. Kac, G. E. Uhlenbeck, and P. C. Hemmer, On the van der Waals Theory of the Vapor-Liquid Equilibrium. I. Discussion of a One-Dimensional Model, *Journal of Mathematical Physics* **4**, 216 (1963).

[81] A. Actor, Evaluation of multidimensional linear zeta functions, *Journal of Number Theory* **35**, 62 (1990).

[82] S. Ravets, H. Labuhn, D. Barredo, L. Béguin, T. Lahaye, and A. Browaeys, Coherent dipole-dipole coupling between two single Rydberg atoms at an electrically-tuned Förster resonance, *Nature Phys* **10**, 914 (2014).

[83] M. D. Lukin, M. Fleischhauer, R. Cote, L. M. Duan, D. Jaksch, J. I. Cirac, and P. Zoller, Dipole Blockade and Quantum Information Processing in Mesoscopic Atomic Ensembles, *Phys. Rev. Lett.* **87**, 037901 (2001).

[84] G. Evenbly, N. Pancotti, A. Milsted, J. Gray, and G. K.-L. Chan, Loop Series Expansions for Tensor Networks (2025), [arXiv:2409.03108 \[quant-ph\]](https://arxiv.org/abs/2409.03108).

[85] F. Iemini, A. Russomanno, J. Keeling, M. Schirò, M. Dalmonte, and R. Fazio, Boundary Time Crystals, *Physical Review Letters* **121**, 035301 (2018).

[86] J. Dunham and M. Szymanska, Data for "Efficient Time Evolution of 2D Open- Quantum Lattice Models

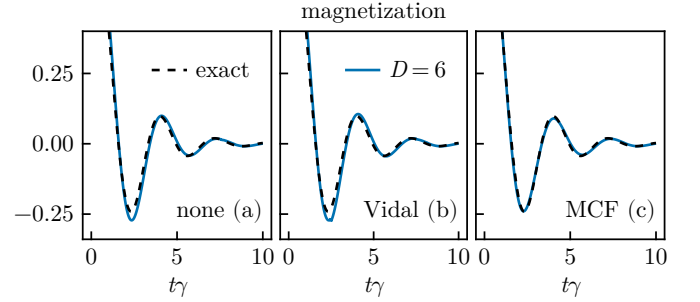


FIG. 12. Effect of gauging fixing on the accuracy of the dissipative Ising model with $J = 1.0$. Plotted alongside is the exact solution (dashed).

with Long-Range Interactions using Tensor Networks", [10.5281/zenodo.17656737](https://doi.org/10.5281/zenodo.17656737) (2025).

[87] A. Acuaviva, V. Makam, H. Nieuwboer, D. Pérez-García, F. Sittner, M. Walter, and F. Witteveen, The minimal canonical form of a tensor network, in *2023 IEEE 64th Annual Symposium on Foundations of Computer Science (FOCS)* (IEEE Computer Society, 2023) pp. 328–362.

[88] E. H. Moore, On the reciprocal of the general algebraic matrix, *Bull. Amer. Math. Soc.* **26**, 394 (1920).

[89] A. Bjerhammar, Rectangular reciprocal matrices, with special reference to geodetic calculations, *Bull. Geodésique* **20**, 188 (1951).

[90] R. Penrose, A generalized inverse for matrices, *Mathematical Proceedings of the Cambridge Philosophical Society* **51**, 406 (1955).

[91] V. Zauner-Stauber, L. Vanderstraeten, M. T. Fishman, F. Verstraete, and J. Haegeman, Variational optimization algorithms for uniform matrix product states, *Phys. Rev. B* **97**, 045145 (2018).

[92] M. T. Fishman, L. Vanderstraeten, V. Zauner-Stauber, J. Haegeman, and F. Verstraete, Faster methods for contracting infinite two-dimensional tensor networks, *Phys. Rev. B* **98**, 235148 (2018).

[93] A. Nietner, B. Vanhecke, F. Verstraete, J. Eisert, and L. Vanderstraeten, Efficient variational contraction of two-dimensional tensor networks with a non-trivial unit cell, *Quantum* **4**, 328 (2020).

[94] P. Corboz, S. R. White, G. Vidal, and M. Troyer, Stripes in the two-dimensional $\pm\pm$ model with infinite projected entangled-pair states, *Phys. Rev. B* **84**, 041108 (2011).

Appendix A: Gauge Fixing

The iterative stage in iterative simple update (itrSU) implicitly moves the state to toward the Vidal gauge in a similar way to the standard simple update procedure over the course of many time-steps. We found that in addition, explicitly gauging the tensor network to the Vidal gauge at each time step had little effect. Interestingly however, we found more accurate results were obtained when fixing the gauge to the so-called *minimal canonical form* described in Ref. [87], when compared to the exactly solvable model (16), as shown in Fig. 12.

| Rule | Index (e, s, w, n) | Value | Rule type |
|------|---------------------------|------------------------------------|-----------|
| | (0, 0, 0, 0) | $\mathbb{1}$ | identity |
| | (0, 0, 0, 0) | $-i\hat{D}$ | D |
| | (0, 0, 2, 0) | $\sqrt{-iJ_1}\hat{X}$ | C |
| | (0, 0, 0, 2) | $\sqrt{-iJ_1}\hat{X}$ | B |
| | (1, 1, 0, 0) | $J_2J_1^{-1}\mathbb{1}$ | A |
| | (0, 1, 2, 0) | $\frac{1}{2}J_2J_1^{-1}\mathbb{1}$ | A |
| | (1, 0, 0, 2) | $\frac{1}{2}J_2J_1^{-1}\mathbb{1}$ | A |
| | (0, 0, 1, 0) | $\sqrt{-iJ_1}\hat{X}$ | B |
| | (0, 0, 0, 1) | $\sqrt{-iJ_1}\hat{X}$ | C |
| | (2, 0, 0, 0) | $\sqrt{-iJ_1}\hat{X}$ | B |
| | (0, 2, 0, 0) | $\sqrt{-iJ_1}\hat{X}$ | C |

TABLE IV. Example of non-zero FSA rules for the real time-evolution of the J_1 - J_2 Ising-type Hamiltonian (8) such that the resulting tePEPO operator has symmetry between the lattice axes. The bond dimension operator is now $\eta_h = \eta_v = \eta = 3$ for all virtual bonds. We assume $J_1 > 0$, however to treat $J_1 = 0$, remove the two rules in the second group and set $J_1 = 1$. These rules should be used in combination with Table II and Algorithm 1.

Appendix B: Additional FSA Examples

1. Symmetric rules for the J_1 - J_2 Hamiltonian

The FSA rules that generate a given Hamiltonian are not unique. For example, the J_1 - J_2 Hamiltonian (8) can be represented using a tePEPO that is symmetric about both lattice axis at a cost of increasing the bond dimension by 1 on the vertical axis where the unconventional path is not necessary. These rules are listed in Table IV.

2. Toric code

Hamiltonians with terms that are not strictly two-body can also be represented as FSA. For example, the toric code Hamiltonian with qubits defined on the *edges* of a lattice Λ is given by

$$H_{\text{toric}} = -J \sum_{v \in \Lambda} \left(\prod_{j \in v} \hat{\sigma}_j^x \right) - K \sum_{p \in \Lambda} \left(\prod_{j \in p} \hat{\sigma}_j^z \right), \quad (\text{B1})$$

where $v \in \Lambda$ refers to the four qubits on the edges adjacent to the vertex v , and $p \in \Lambda$ refers to the four qubits on the edges defining the plaquette (face) p of the lattice Λ . The Hamiltonian (B1) has an A/B sublattice checkerboard structure, with time-evolution operator generated by the rules give in Table V.

| Rule | Index (e, s, w, n) | Value | Rule type |
|--------------|---------------------------|---------------------|-----------|
| | (0, 0, 0, 0) | $\mathbb{1}$ | identity |
| Sublattice A | | | |
| | (1, 1, 0, 0) | $\sqrt{-iJ}\hat{X}$ | C |
| | (0, 0, 2, 2) | $\sqrt{-iJ}\hat{X}$ | B |
| | (2, 0, 0, 1) | \hat{Z} | A |
| | (0, 2, 1, 0) | \hat{Z} | A |
| Sublattice B | | | |
| | (1, 1, 0, 0) | $\sqrt{-iK}\hat{Z}$ | C |
| | (0, 0, 2, 2) | $\sqrt{-iK}\hat{Z}$ | B |
| | (2, 0, 0, 1) | \hat{X} | A |
| | (0, 2, 1, 0) | \hat{X} | A |

TABLE V. Example of non-zero FSA rules for the real-time evolution of the toric code Hamiltonian (B1). The resulting tePEPO has an A/B sublattice checkerboard structure with bond dimension $\eta = 3$ on both lattice directions. These rules should be used in combination with Table II and Algorithm 1.

Appendix C: Explicit Construction of Vectorized Super-Operators

Neglecting one-local terms for convenience, consider operators of the form

$$H = \sum_{i, j \in \Lambda} \hat{C}_i \hat{B}_j. \quad (\text{C1})$$

Under vectorization, the coherent part of the Lindblad master equation becomes:

$$-i[H, \rho] \xrightarrow{\text{vec}} \left[\sum_{i, j \in \Lambda} \left(\hat{C}_j^{[+]} \hat{B}_k^{[+]} + \hat{C}_j^{[-]} \hat{B}_k^{[-]} \right) \right] |\rho\rangle\langle \rho|. \quad (\text{C2})$$

where we have defined the following terms on the Liouville space:

$$\hat{C}_j^{[+]} \hat{B}_k^{[+]} = -i(\mathbb{1} \otimes \hat{C})_j (\mathbb{1} \otimes \hat{B})_k, \quad (\text{C3})$$

$$\hat{C}_j^{[-]} \hat{B}_k^{[-]} = i(\hat{C}^\top \otimes \mathbb{1})_j (\hat{B}^\top \otimes \mathbb{1})_k, \quad (\text{C4})$$

Each two-body term then contributes a value of 2 to the bond dimension per term in the Hamiltonian. Dissipation between different lattice sites can be treated by writing the terms in the dissipator a sum of distinct operators. Consider the two-body Lindblad operator $\hat{L}_{i,j} = \sqrt{\gamma} \hat{\Gamma}_i \hat{\Gamma}_j$ acting on sites i and j . Under vectorization, this gener-

ates the following three two-body terms terms:

$$\hat{C}_j^{[1]} \hat{B}_k^{[2]} = \gamma(\hat{\Gamma}^* \otimes \hat{\Gamma})_j (\hat{\Gamma}^* \otimes \hat{\Gamma})_k, \quad (\text{C5})$$

$$\hat{C}_j^{[2]} \hat{B}_k^{[2]} = -\frac{\gamma}{2} (\mathbb{1} \otimes \hat{\Gamma}^\dagger \hat{\Gamma})_j (\mathbb{1} \otimes \hat{\Gamma}^\dagger \hat{\Gamma})_k, \quad (\text{C6})$$

$$\hat{C}_j^{[3]} \hat{B}_k^{[3]} = -\frac{\gamma}{2} (\hat{\Gamma}^\top \hat{\Gamma}^* \otimes \mathbb{1})_j (\hat{\Gamma}^\top \hat{\Gamma}^* \otimes \mathbb{1})_k, \quad (\text{C7})$$

which can be represented using FSA in the same way as done with Hamiltonian terms. In general, each non-purely-local Lindblad operator thus contributes a value of 3 to the total bond-dimension of the resulting tensor-network time-evolution operator. The total generator of the time evolution can then be expressed as

$$\mathcal{G} = \sum_{i,j \in \Lambda} \left[\sum_k \left(\hat{C}_i^{[k,+]} \hat{B}_j^{[k,+]} + \hat{C}_i^{[k,-]} \hat{B}_j^{[k,-]} \right) + \sum_q \sum_{\alpha=1}^3 \hat{C}_i^{[q,\alpha]} \hat{B}_j^{[q,\alpha]} \right]. \quad (\text{C8})$$

1. Thermal State Evolution

Imaginary time evolution of a thermal state can be represented in a similar way to Lindblad real-time evolution. A finite temperature state $\rho(\beta)$ can be expressed in terms of the Hamiltonian H as

$$\rho(\beta + \delta\beta) = e^{-\frac{\delta\beta}{2} H} \rho(\beta) e^{-\frac{\delta\beta}{2} H}, \quad (\text{C9})$$

where $\beta = 1/k_B T$ is the thermodynamic beta in terms of temperature T and Boltzmann constant k_B . The vectorized from of the generator of the evolution (C9) is then given by

$$\mathcal{G}_{\text{th}} = -\frac{1}{2} (\mathbb{1} \otimes H + H^\top \otimes \mathbb{1}). \quad (\text{C10})$$

Therefore, by defining:

$$\hat{C}_j^{[k]} \hat{B}_k^{[k]} = -\frac{1}{2} (\mathbb{1} \otimes \hat{C})_j (\mathbb{1} \otimes \hat{B})_k, \quad (\text{C11})$$

$$\hat{C}_j^{[b]} \hat{B}_k^{[b]} = -\frac{1}{2} (\hat{C}^\top \otimes \mathbb{1})_j (\hat{B}^\top \otimes \mathbb{1})_k, \quad (\text{C12})$$

the generator of the time-evolution can be expressed as

$$\mathcal{G}_{\text{th}} = \sum_{i,j \in \Lambda} \left[\sum_k \left(\hat{C}_i^{[k,k]} \hat{B}_j^{[k,k]} + \hat{C}_i^{[k,b]} \hat{B}_j^{[k,b]} \right) \right], \quad (\text{C13})$$

with an additional arbitrary number of local terms that do not contribute to the bond dimension.

Appendix D: Iterative Simple Update

Assuming the tePEPO time-evolution super operator has been applied to each iPEPO tensor in the lattice,

then the the itrSU method is summarized as follows: Assume each bond $\alpha = (u, v)$ was truncated in the previous time-step by isometries U_α and V_α where U_α truncates the tensors at u and V_α truncates the tensors at v . Then each tensor at v as an isometry $V_{u,\beta}^{[0]}$ associated to each bond β incident to u that was used to reduce the dimension of associated index of the tensors A_v in the previous timestep. Then the n -th iteration of itrSU proceeds as follows:

1. For bond $\alpha = (u, v)$, form the tensors P_A and P_B by respectively applying isometries $V_{u,\beta}^{[n-1]}$ on A_u and $V_{v,\gamma}^{[n-1]}$ on A_v for bonds $\beta, \gamma \neq \alpha$, i.e. truncate the bonds of A_u and A_v excluding bond α .
2. Perform *parallel simple update*, i.e.
 - (a) absorb the square root of the weights $\lambda^{[n-1]}$ on bonds $\beta, \gamma \neq \alpha$ into the appropriate tensors.
 - (b) decompose tensors $P_A = Q_A M_A$ and $M_B Q_B = P_B$ using the QR decomposition, where the indices are grouped such that the only bonds in domain (codomain) of P_A (P_B) are α .
 - (c) perform a truncated singular value decomposition on the product $M_A M_B$ to obtain isometries and new bond weight:

$$M_A M_B \xrightarrow{\text{SVD}_D} U \lambda_\alpha^{[n]} V^\dagger \quad (\text{D1})$$

- (d) construct the isometries:

$$\tilde{U} = M_A^+ U \sqrt{\lambda_\alpha^{[n]}}, \quad (\text{D2})$$

$$\text{and } \tilde{V} = \sqrt{\lambda_\alpha^{[n]}} V M_B^+, \quad (\text{D3})$$

where M^+ is the pseudo-inverse of M [88–90].

3. Set new isometries $V_{u,\alpha}^{[n]} = \tilde{U}$ and $V_{v,\alpha}^{[n]} = \tilde{V}^\dagger$ and bond weight $\lambda_\alpha^{[n]}$.
4. Repeat steps 1–3 for each bond in the lattice.

This process is repeated until singular values $\lambda_\alpha^{[n]}$ converge to desired threshold. Finally, once converged, truncated tensors \tilde{A}_v are formed by truncating each bond of each tensor with $V_{v,\alpha}^{[n]}$.

The itrSU method can be performed in parallel, where each site in the lattice is update independently at each iteration, or in sequence, where the isometries obtained from truncating a bond are used in subsequent truncations during the same iterative cycle. The former is useful for maintaining lattice symmetries assuming a symmetric time-evolution operator. We find consistent convergence is found using parallel itrSU with a tolerance on the order of $\sim 1 \times 10^{-8}$.

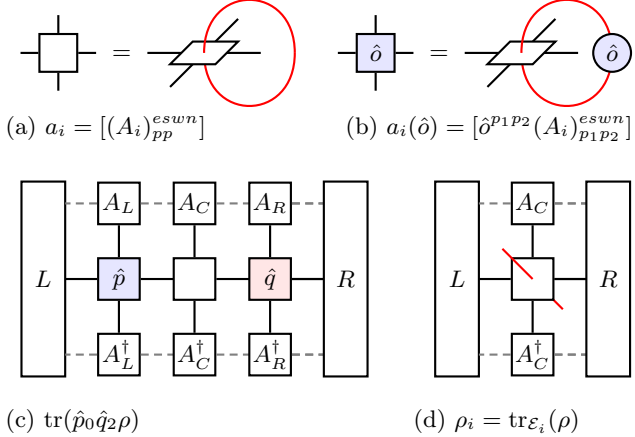


FIG. 13. (c) Example of how to compute a next-nearest neighbor correlation function using boundary MPS $|\Psi(\{A_C, A_L, A_R\})\rangle$ and transfer matrix fixed points L and R obtained from applying the VUMPS procedure to the network formed from the rank-4 tensors $\{a\}$ defined in (a). In (d), the construction of a reduced density matrix is shown. The partial trace of the infinite lattice is approximated by an environment with finite bond-dimension χ shown by the dashed lines.

Appendix E: VUMPS

To compute $\text{tr}(\rho)$, one must contract the entire infinite tensor network, including physical indices. As this is not possible exactly, one uses an appropriate renormalization group or boundary algorithm to approximate

this contraction. In the context of computing observables, boundary methods are more suitable as it is more straightforward to embed non-translationally invariant tensors in the partially contracted tensor network. This is useful to, for example, construct reduced density matrices by embedding an intact iPEPO tensor A_i whose physical indices are to remain *un-traced* into a trace environment, \mathcal{E}_i shown in Fig. 4b, represented by the boundary tensors.

The method used in this is the paper is VUMPS algorithm [91], adapted to the generic task of computing contractions of infinite two-dimensional tensor networks [92, 93]. The output of VUMPS is a boundary MPS $|\Psi(\{A_C, A_L, A_R\})\rangle$ with bond-dimension χ that approximates the contraction of the upper and lower infinite portions of the lattice, and left and right fixed points L and R of the transfer matrices:

$$T_L := \begin{array}{c} \text{---} [A_L] \text{---} \chi \\ | \\ \text{---} [] \text{---} D \end{array} \text{, and } T_R := \begin{array}{c} \text{---} [A_R] \text{---} \chi \\ | \\ \text{---} [] \text{---} D \end{array} \text{, (E1)}$$

$$\text{---} [A_L^\dagger] \text{---} \chi \qquad \qquad \text{---} [A_R^\dagger] \text{---} \chi$$

i.e. $L T_L = L$ and $T_R R = R$.

In Fig. 13 we show how to compute the n -point correlation function $\langle \hat{p}_0 \hat{q}_2 \rangle$, and a single site reduced density matrix using the VUMPS boundary tensors. Correlation functions between sites diagonal to each other are not compatible with VUMPS. In that case one can make use of an alternative method such as the corner transfer matrix renormalization group [92, 94].